MONOGRAPHS IN ELECTRICAL AND ELECTRONIC ENGINEERING • 30

Linear Induction Drives

JACEK F. GIERAS

OXFORD SCIENCE PUBLICATIONS

Monographs in Electrical and Electronic Engineering

Series editors: P. Hammond, T. J. E. Miller, and S. Yamamura

Monographs in Electrical and Electronic Engineering

10. *The theory of linear induction machinery* (1980) Michel Poloujadoff
12. *Energy methods in electromagnetism* (1981) P. Hammond
15. *Superconducting rotating electrical machines* (1983) J. R. Bumby
16. *Stepping motors and their microprocessor controls* (1984) T. Kenjo
17. *Machinery noise measurement* (1985) S. J. Yang and A. J. Ellison
18. *Permanent-magnet and brushless d.c. motors* (1985) T. Kenjo and S. Nagamori
19. *Metal-semiconductor contacts. Second edition* (1988) E. H. Rhoderick and R.H. Williams
20. *Introduction to power electonics* (1988) Eiichi Ohno
21. *Brushless permanent-magnet and reluctance motor drives* (1989) T. J. E. Miller
22. *Vector control of a.c. machines* (1990) Peter Vas
23. *Brushless servomotors: fundamentals and applications* (1990) Y. Dote and S. Kinoshita
24. *Semiconductor devices, circuits, and systems* (1991) Albrecht Möschwitzer
25. *Electrical machines and drives: a space-vector theory approach* (1992) Peter Vas
26. *Spiral vector theory of a.c. circuits and machines* (1992) Sakae Yamamura
27. *Parameter estimation, condition monitoring, and diagnosis of electrical machines* (1993) Peter Vas
28. *An introduction to ultrasonic motors* (1993) S. Sashida and T. Kenjo
29. *Ultrasonic motors: theory and applications* (1993) S. Ueha and Y. Tomikawa
30. *Linear induction drives* (1993) J. F. Gieras
31. *Switched reluctance motors and their controls* (1993) T. J. E. Miller
32. *Numerical modelling of eddy currents* (1993) Andrzej Krawczyk and John A. Tegopoulos

Linear Induction Drives

Jacek F. Gieras

Professor of Electrical Machines

CLARENDON PRESS · OXFORD

1994

Oxford University Press, Walton Street, Oxford OX2 6DP
Oxford New York Toronto
Delhi Bombay Calcutta Madras Karachi
Kuala Lumpur Singapore Hong Kong Tokyo
Nairobi Dar es Salaam Cape Town
Melbourne Auckland Madrid
and associated companies in
Berlin Ibadan

Oxford is a trade mark of Oxford University Press

Published in the United States
by Oxford University Press Inc., New York

A catalogue record for this book is available from the British Library

Library of Congress Cataloging in Publication Data
ISBN 0 19 859381 3

Typeset by the author using LaTeX

Printed in Great Britain by
Biddles Ltd, Guildford & King's Lynn

CONTENTS

PRINCIPAL SYMBOLS

$\mathbf{A}$ magnetic vector potential

A line current density; surface

$\mathbf{a}$ operator $\mathbf{a} = \exp(j2\pi/3)$

a instantaneous value of the line current density

a_R coefficient taking into account the nonlinear magnetic permeability and hysteresis losses in calculating the resistance and active power loss

a_X coefficient taking into account the nonlinear magnetic permeability and hysteresis losses in calculating the reactance and reactive power loss

B magnetic flux density

b instantaneous value of the magnetic flux density; width of slot

C capacitance

c_1 width of a tooth of the primary core

D diameter; damping (friction) coefficient

d thickness of the highly conducting layer; thickness of the secondary of a double-sided LIM; height or diameter of the secondary conductor (bar)

E electric field intensity; electromotive force (EMF); induced voltage

F force

f frequency; force per unit area

g airgap (mechanical clearance)

g_t total airgap

H magnetic field intensity

h height

h_{sec} thickness of the secondary ferromagnetic core (back iron)

I current; functional

i instantaneous value of the current

J current density

j imaginary unit $j = \sqrt{-1}$

K stiffness coefficient

k_C Carter's coefficient

k_e longitudinal end effect factor

k_{sat} saturation factor of the magnetic circuit due to the main (linkage) magnetic flux

k_Q goodness factor

k_{RN} factor for reducing the secondary conductivity due to transverse edge effects (modified Russell and Norsworthy factor)

k_{tr} turns ratio for reducing the secondary impedance to the primary winding

k_u imbalance factor

k_w winding factor

k_z factor for increasing the secondary impedance due to transverse edge effects

k_ν attenuation factor of the electromagnetic field in the secondary for the νth space harmonic

L self-inductance

L_i effective width of the primary core

L_τ length of the primary core (along the pole pitch)

M mutual inductance

m number of phases; mass

N number of turns per phase

n time harmonic

P active power

p number of pole pairs

Q number of slots per pole; reactive power

q number of slots per pole per phase

R resistance

r radius

S apparent power

s slip

s_{cr} critical slip corresponding to maximum (pull-out) electromagnetic thrust F_{max}

str stray loss

t time; slot pitch

t_{ov} thickness of highly conducting layer behind the secondary core (back iron)

V electric voltage; volume

v instantaneous value of the electric voltage

V_μ magnetic voltage

v velocity of the secondary in the x direction

v_s synchronous velocity

w width of the secondary (core)

w_c coil pitch

w_{ov} width of the highly conducting layer behind the secondary ferromagnetic core (back iron)

X reactance

x, y, z Cartesian coordinates

$\mathbf{Z}$ impedance $\mathbf{Z} = R + jX$

z number of slots

α angle between currents in neighbouring bars of a cage winding

α_i *average value-to-maximum value* ratio of the magnetic flux density

β real constant $\beta = \pi/\tau$

$\beta_{A,B,C}$ angle between phase voltages

β_ν real constant $\beta_\nu = \nu\pi/\tau$ dependent on the space harmonic order ν

η efficiency

Θ magnetomotive force (MMF); coordinate of cylindrical system

ϑ instantaneous value of the magnetomotive force

κ_{sat} saturation factor of the magnetic circuit due to leakage magnetic fluxes

κ_ν complex propagation constant for the νth space harmonic dependent on the pole pitch

λ coefficient of leakage permeance (specific leakage permeance)

μ magnetic permeability

μ_o magnetic permeability of free space $\mu_o = 0.4\pi \times 10^{-6}$ H/m

μ_r relative magnetic permeability

μ_{re} complex equivalent relative magnetic permeability

ν space harmonic of the field distribution along the pole pitch

ξ reduced height of the conductor

σ electric conductivity

σ_f form factor

τ pole pitch

Φ magnetic flux

ϕ phase angle between current and voltage

Ψ linkage magnetic flux

Ω angular speed $\Omega = 2\pi n$

ω angular frequency $\omega = 2\pi f$

Subscripts

Al highly conductive material (aluminium)

av average

b bar of cage (ladder) winding

cag cage (ladder) winding

d differential

e equivalent; end connection (segment of the side bar)

Fe ferromagnetic core

i number of the subsequent layer

in input

m peak (maximum) value

n nth time harmonic

out output

ov overhang (end connection)

r, Θ, x projections of a vector on cylindrical coordinates r, Θ, x

s surface value; slot

str stray loss

u, v rectangular coordinates moving with any velocity v_k

x, y, z projections of a vector on rectangular coordinates x, y, z

ν νth space harmonic

1 primary

2 secondary

Superscripts

+ positive-sequence component; forward-travelling field

− negative-sequence component; backward-travelling field

(i) number of layers of which the secondary is composed

1

REVIEW OF CONSTRUCTION

Linear electric motors belong to the group of special electrical machines that convert electrical energy directly into mechanical energy of translatory motion. Linear electric motors can be classified as follows:

- d.c. motors,
- induction motors,
- synchronous motors, including reluctance and stepping motors,
- oscillating motors,
- hybrid motors.

The most popular are linear induction motors (LIMs), which are manufactured commercially in several countries and are finding many applications.

1.1 History

The concept of linear electric motors is more than 150 years old. The first proposal was patented in 1841 (Wheatstone).[79, 81, 142] The first LIM was patented in 1890.[115] A lot of patents on the use of LIMs in *textile shuttle* propulsion appeared between 1895 and 1940. In 1905 two projects for applications of LIMs to traction were proposed.[81] In 1923 a *moving pavement* for pedestrians propelled by a flat LIM along 42nd Street from Grand Central Terminal to Times Square in New York was designed.[81] The construction of a flat, single-sided LIM with a synchronous velocity of 100 m/s to be used to accelerate starting airplanes, by the Westinghouse Company of America in 1945, was an important event in the development of LIMs.[79, 81] This apparatus, called *'Electropult'* could develop an initial starting thrust of 75 600 N and accelerate a mass of 5 000 kg to a speed of 185 km/h in a distance of 160 m in 4.2 s. The short primary had a three-phase winding and the long secondary (1 600 m) was also wound. After taking off (input phase current 7 kA), the primary was disconnected from the three-phase power supply and decelerated by applying dynamic braking (input d.c. current 10 kA).

Progress in construction of nuclear reactors demanded efficient *pumps for liquid metals* like sodium, sodium–potassium alloy, and bismuth. In the late 1950s induction pumps for liquid metals were designed.[139, 141] In

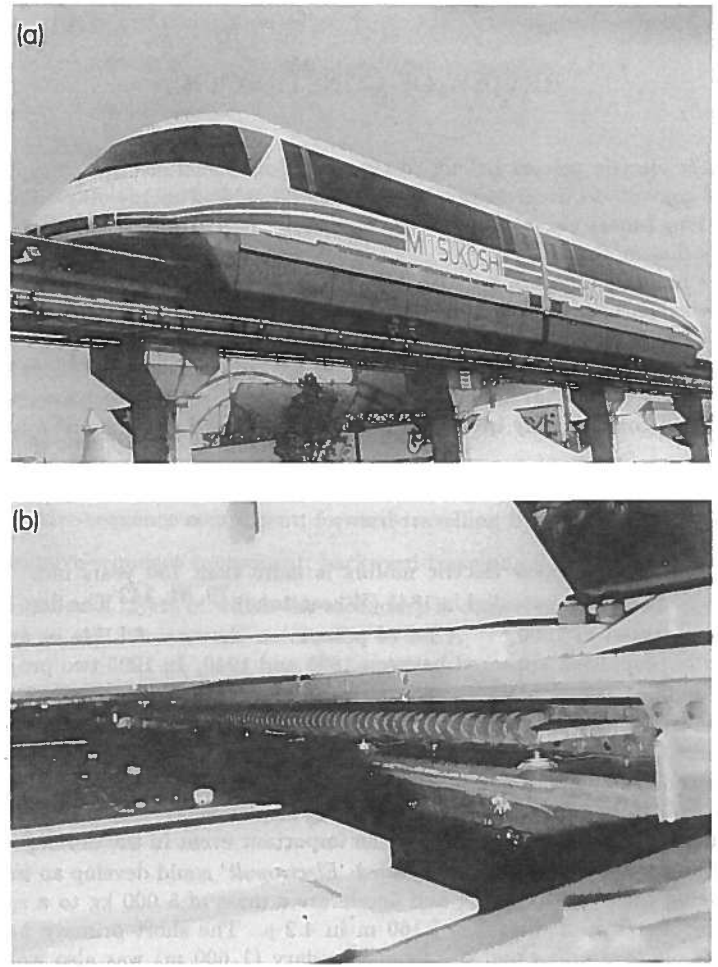

FIG. 1.1. The HSST-05 magnetic levitation train: (a) general view; (b) single-sided LIM for propulsion. (Photo courtesy of HSST Corporation, Japan.)

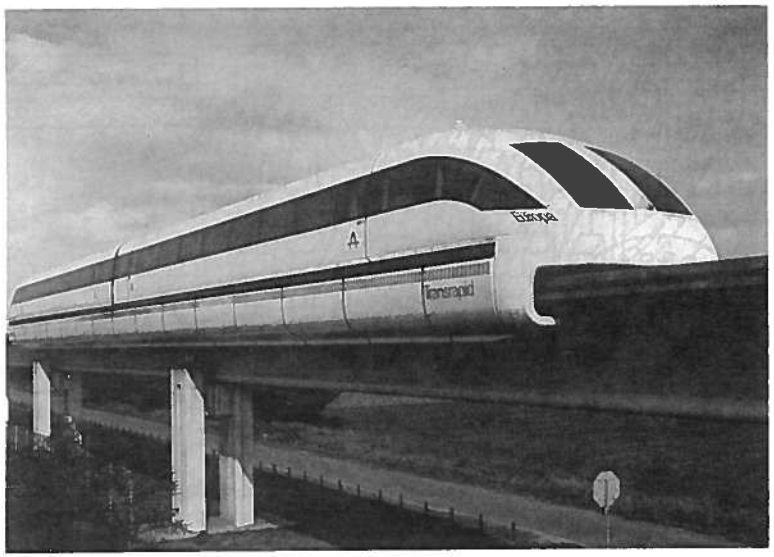

FIG. 1.2. The Transrapid 07 magnetic levitation train. (Photo courtesy of Thyssen Henschel, Germany.)

the early 1960s induction pumps for the *transportation of melted steel* in ironworks were designed.[138]

In the 1960s various devices for the *simulation of car collisions* were also worked out, with tested cars being accelerated to 100 km/h.[95, 142]

There was a great deal of interest in *high-speed transportation systems*, that is, *magnetic levitation systems*, in the 1970s (Figs. 1.1, 1.2). Vehicles that are suspended magnetically can reach speeds of more than 500 km/h and can be propelled either by synchronous linear motors or by LIMs.[1, 9, 95, 142] Also, application of LIMs to *wheel-on-rail traction cars* can offer advantages since, amongst other things, propulsion and braking are independent of *adhesion*.[130, 140]

LIMs have found the widest prospects for applications in *transportation systems*, beginning with electrical traction on small passenger or material supply cars (used at airports, exhibitions, electrohighways, elevators) and ending with pallet transportation, wafer transportation, belt conveyors, transportation systems of bulk materials, etc. The second important place for LIM applications is in industry, i.e. *manufacturing processes* (machine tools, hammers, presses, mills, separators, automated manufacturing sys-

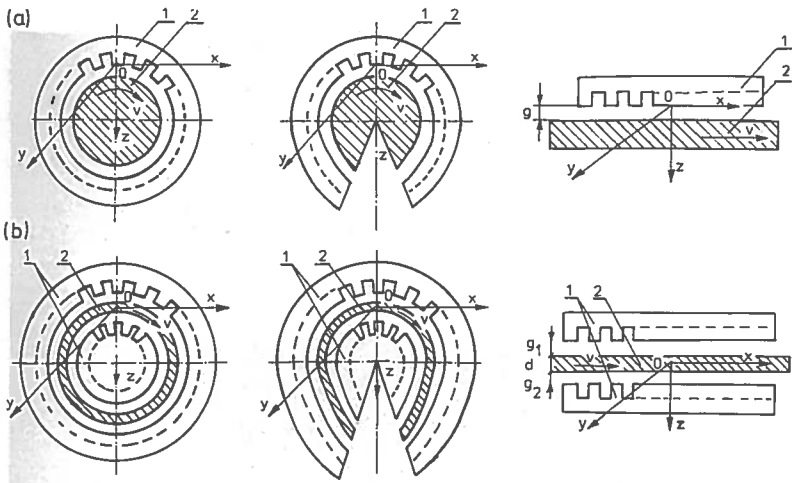

FIG. 1.3. Evolution of a rotary induction motor: (a) solid rotor induction motor into a flat, single-sided LIM, (b) hollow-rotor induction motor into a flat double-sided LIM: 1 — primary, 2 — secondary.

tems, strip tensioners, textile shuttles, index tables, turntables, disc saws for wood, sliding doors, robots, etc.) LIMs can also play an important part in *industrial investigations and tests*, e.g. high acceleration of model aircraft in aerodynamic tunnels, high acceleration of vessels in laboratory pools, propulsion of mixers, shakers and vibrators, adjusting $x - y$ tables and instruments, etc. There is also a possibility of using LIMs in *consumer electronics* (sound and vision equipment, knitting machines, curtains) and in *offices* (transportation of documents, letters, and cash). The *'Handbook of linear motor applications'* [142] printed in Japan in 1986 contains about 50 examples of applications of LIMs in operation or in the process of implementation.

There are a lot of research and development centres carrying out research on LIMs, the majority of them in Europe, Japan, and Northern America.

1.2 Geometry and classification

A linear motor can be obtained by cutting a rotary motor along its radius from the centre axis of the shaft to the external surface of the stator core and rolling it out flat. A LIM can be obtained by cutting in the same way either a cage rotor induction motor or a wound rotor induction motor. The

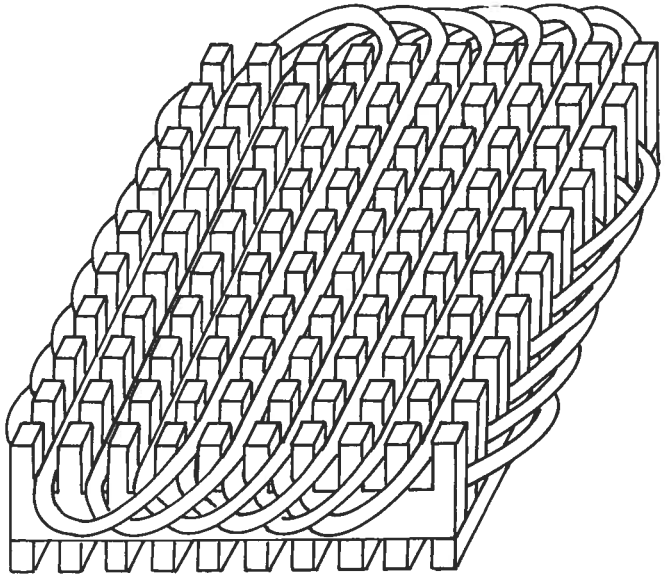

FIG. 1.4. The primary of a flat LIM with two degrees of freedom.

stator becomes the *primary* and the rotor becomes the *secondary*. The secondary of a LIM can be simplified by using a solid steel core and replacing the cage (ladder) or slip-ring winding with a high-conductivity nonferromagnetic plate (aluminium or copper). The nonferromagnetic plate is a secondary electric circuit with distributed parameters, and the ferromagnetic core is a conductor both for the magnetic flux and the electric current. It does not matter from the principle of operation point of view which part (primary or secondary) is in motion. Thus, the *flat, single-sided LIM* can be obtained from a solid rotor induction motor (Fig. 1.3a) and the *flat, double-sided LIM* can be obtained from a hollow-rotor induction motor with wound external and internal stator (Fig. 1.3b). In a double-sided LIM the secondary ferromagnetic core is not necessary, since the magnetic flux excited by one of the primary windings after passing through the airgaps and nonferromagnetic secondary is then closed up by the core of the second primary.

Theoretically, a *double-sided LIM* with primary windings located on two cores, in comparison with a single-sided LIM exciting the same MMF, has twice the airgap magnetic flux density. Therefore, the *thrust* of such a motor is four times greater, assuming the same dimensions.[115] If only one

Table 1.1 *Design data of small, single-sided, three-phase LIMs*

Quantity	LIM		Unit
	SL-5-100	SL-5-270	
Thrust at $s = 1$, F_x	$\geq$ 100.0	$\geq$ 270.0	N
Input frequency, f	50.0	50.0	Hz
Input phase voltage, V_1	220.0	220.0	V
Number of poles, $2p$	4	4	–
Number of turns per phase, N_1	840	420	–
Number of compensating turns per phase, N_{1c}	140	70	–
Diameter of conductor, d_1	0.75	1.10	mm
Effective width of primary core, L_i	0.05	0.10	m
Pole pitch, τ	0.05	0.05	m
Length of single end connection, l_e	0.12	0.12	m
Coil pitch, w_c	0.05	0.05	m
Airgap, g	1 to 2	1 to 2	mm
Number of slots, z_1	12	12	–
Width of slot, b_{11}	10.2	10.2	mm
Width of slot opening, b_{14}	8.0	8.0	mm
Depth of slot, h_1	45.0	45.0	mm
Height of yoke, h_{1y}	31.0	31.0	mm
Conductivity of solid secondary core at 20^{0}C, σ_{Fe}	4.5 to 6.5	4.5 to 6.5	$\times 10^6$ S/m
Conductivity of aluminium cap at 20^{0}C, σ_{Al}	$\approx$ 30.0	$\approx$ 30.0	$\times 10^6$ S/m
Width of secondary core, w	$\geq$ 0.05	$\geq$ 0.10	m
Thickness of secondary core, h_{sec}	$\geq$ 5.0	$\geq$ 5.0	mm
Thickness of aluminium cap, d	3.0	3.0	mm

primary core is wound the output parameters of a double-sided LIM are the same as those for a single-sided LIM with laminated secondary back iron.[143] The fundamental advantage of double-sided LIMs is the elimination of the normal attractive force between the primary and the secondary, because the secondary is usually nonferromagnetic.

The design data of low-power LIMs manufactured in Poland are presented in Table 1.1.

Flat LIMs can have primary cores consisting of an array of cores arranged in parallel at appropriate distances and connected magnetically by additional yokes perpendicular to the direction of the travelling field. A magnetic circuit designed in such a way makes it possible to apply two windings, in general multi-phase windings, with perpendicular conductors,[142] as shown in Fig. 1.4. Adjusting the current in each winding, the secondary can be moved in two perpendicular directions and can be positioned at any point of the $x - y$ plane. A *flat LIM with two degrees of freedom* can be designed both as a single-sided and a double-sided machine.

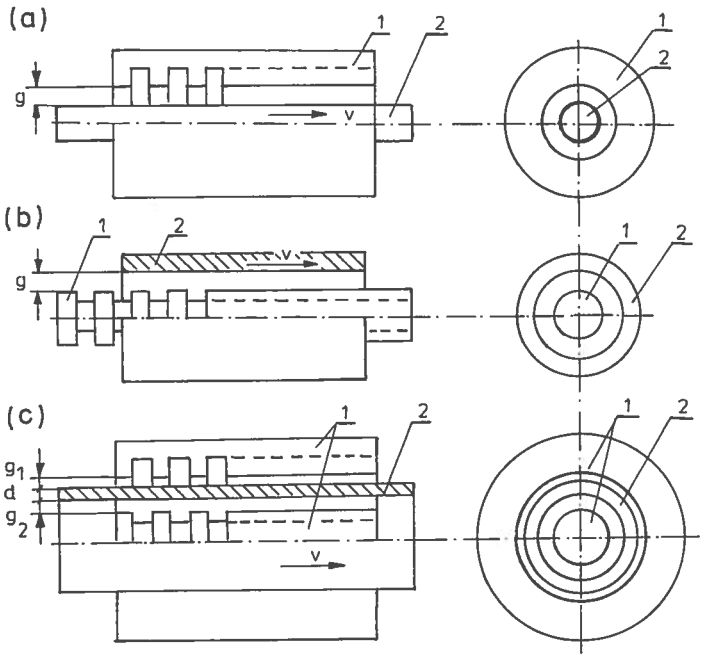

FIG. 1.5. Tubular LIMs: (a) single-sided with an external short primary, (b) single-sided with an external short secondary, (c) double-sided with short primary. 1 — primary, 2 — secondary.

By rolling a flat, single-sided or double-sided LIM around the axis parallel to the direction of the travelling magnetic field, i.e. parallel to the direction of the thrust, a tubular motor can be obtained (Fig. 1.5).

A *tubular (cylindrical) LIM*, similar to a flat LIM, can be designed both as a single-sided and a double-sided machine and can have a square, or rectangular cross-section,[144] as in Fig. 1.6. There are possible configurations other than that in Fig. 1.6, regarding the length of the secondary with respect to the length of the primary.

The design data of some tubular LIMs with cylindrical cross-section manufactured by Demag Fördertechnik Antriebstechnik, Hamburg, Ger-

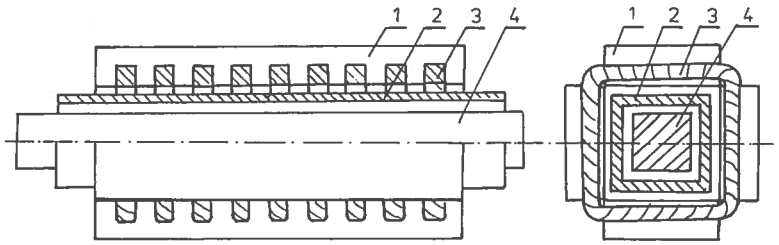

FIG. 1.6. Tubular, double-sided LIM with a square cross-section: 1 — primary, 2 — secondary, 3 — primary coil, 4 — internal core.

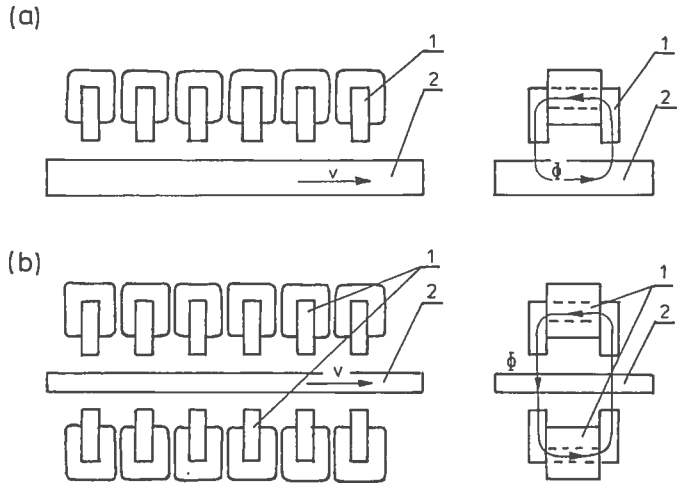

FIG. 1.7. Flat LIM with transverse magnetic flux and salient poles: (a) single-sided, (b) double-sided. 1 — primary, 2 — secondary.

many, are presented in Table 1.2. According to *International Electrotechnical Commission (IEC)* standards, S1 means continuous running duty and S2 means short-time duty (IEC Publication 34-1).

All the above-mentioned LIMs are motors with *longitudinal magnetic flux*, i.e. the lines of magnetic flux lie in the plane parallel to the direction of the travelling magnetic field. A LIM can also be designed in such a way as to obtain magnetic flux lines perpendicular to the direction of the travelling

Table 1.2 *Data of small three-phase tubular LIMs*

Duty type	Quantity	LIM			Unit
		LMP 19/12	LMP 19/18	LMP 19/24	
S1	Thrust at $s = 1$, F_x	10.0	12.0	13.0	N
	Input phase current, I_1	0.23	0.27	0.28	A
	Input power, P_{in}	120	145	160	W
S2	Thrust at $s = 1$, F_x	150...16	230...19	315...21	N
	Input phase current, I_1	8.2...0.37	10.5...0.4	12.5...0.5	A
	Input power, P_{in}	3.2...0.18	5.0...0.20	5.9...0.22	kW
	Duty time	10...1800	10...1800	10...1800	s
Rated input phase voltage, V_{1r}			220		V
Connection			Y		-
Input frequency, f			50		Hz
Synchronous velocity, v_s			3.9		m/s
Class of insulation			F		-
Secondary diameter			19		mm
Secondary mass			0.48...1.28		kg
Secondary length			0.28...0.75		m
Max. temperature of secondary			115		^{0}C
Mass of primary		4.2	5.7	7.2	kg
Number of primary coils		12	18	24	-

field.[35, 38, 42, 115] Such motors are said to have *transverse magnetic flux* (Fig.1.7).

The fundamental advantage of a LIM with transverse magnetic flux in comparison with a LIM with longitudinal magnetic flux is the lower magnetizing current necessary, due to the shorter magnetic flux paths. The significant disadvantage is lower thrust. A flat LIM with transverse magnetic flux usually has a primary winding of concentrated coils located on salient poles.

A flat, single-sided LIM with transverse flux can produce not only thrust but also *electrodynamic suspension*. In the design shown in Fig. 1.8 the secondary is suspended electrodynamically, and propelled and stabilized laterally by the primary magnetic field.[35] The primary magnetic circuit consists of E-shaped laminations assembled in two rows. The short sec-

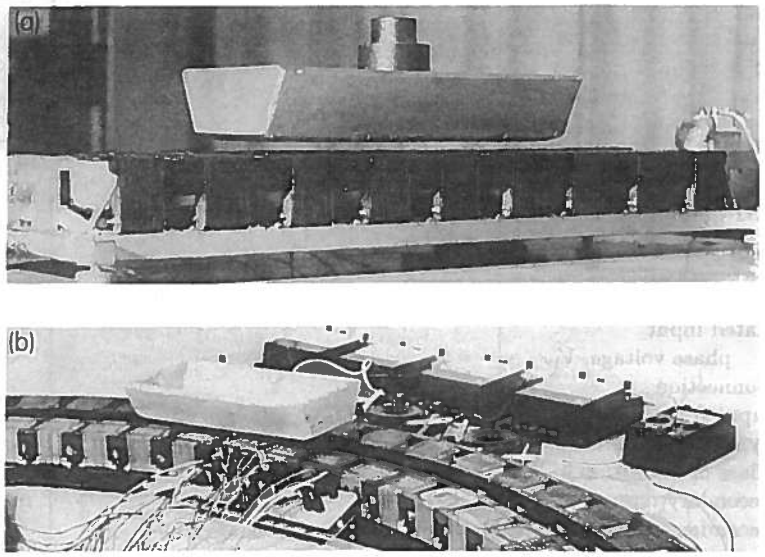

FIG. 1.8. Flat LIM with transverse magnetic flux, salient poles, and nonferromagnetic secondary propelled, suspended, and stabilized electrodynamically: (a) straight primary, (b) arc-shaped primary.

ondary is made of light aluminium alloy in the form of a boat. The lateral sides of the boat are inclined by 60^0 with respect to the active surface. Such a shape provides maximum normal repulsive force and maximum lateral stabilization.

In a similar way a flat LIM with salient poles and longitudinal magnetic flux (Fig. 1.9) can be designed to obtain electrodynamic suspension, propulsion, and stabilization.[51, 59] The long primary consists of three-phase electromagnets assembled in two rows. The short secondary (vehicle) consists of three parallel parts in the shape of boats creating a *threemaran*. Such a LIM was invented by P. Hochhäusler (German patent No. 2422083/1980).

In this section only typical and the most popular configurations of LIMs have been described. Special designs are discussed in Chapter 5.

According to their geometry, the LIMs can be divided into the following groups:

- with movable primary or movable secondary,

FIG. 1.9. Flat LIM with longitudinal magnetic flux, salient poles, and nonferromagnetic secondary propelled, suspended, and stabilized electrodynamically (German patent No. 2422083/1980).

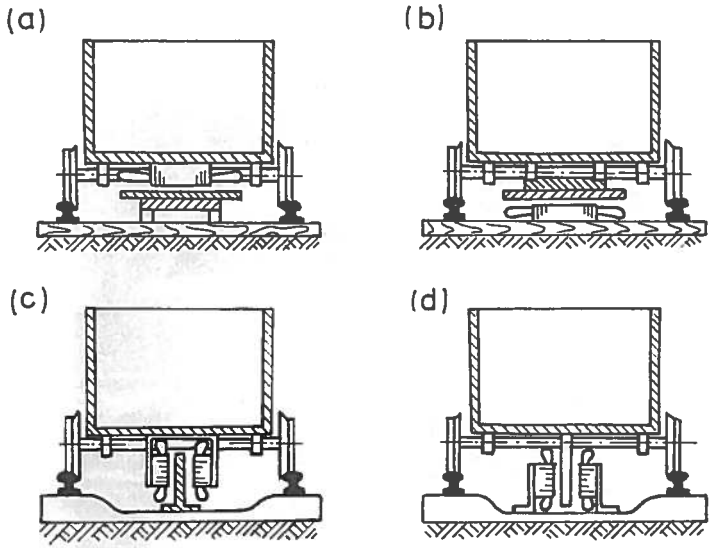

FIG. 1.10. LIM-driven wheel-on-rail cars: (a) single-sided LIM with short primary mounted on the undercarriage, (b) single-sided LIM with short secondary mounted on the undercarriage, (c) double-sided LIM with short primary mounted on the undercarriage, (d) double-sided LIM with short secondary mounted on the undercarriage.

- single-sided and double-sided,
- flat and tubular,
- with short primary and short secondary,
- with longitudinal and transverse magnetic flux.

1.3 Propulsion of wheel-on-rail vehicles

Modern railway systems and electrical traction should meet the following requirements:

- high level of automatization and computerization;
- propulsion and braking independent of adhesion which in turn is affected, first of all, by climate and weather;
- low level of noise, sometimes below 70 dB (A);
- ability to cope with high slopes, at least 6%, and sharp bends with radius of curvature less than 20 m;
- no pollution to natural environtment and landscape;
- high reliability.

Table 1.3 *Design data of single-sided, three-phase LIMs for propulsion of vehicles*

Quantity	LIM					Unit
	JLMDR	ICTS	KU	CIGGT	GEC	
Pull-out thrust at frequency given below, F_x	12.5	9.0	3.5	1.7	0.7	kN
Input frequency, f	20.0	40.0	25.0	40.0	60.0	Hz
Rated phase current, V_1	275.0	465.0	130.0	200.0	200.0	A
Number of poles, $2p$	8	6	4	6	4	–
Number of turns per phase, N_1	128	96	128	108	48	–
Equivalent diameter of conductor, d_1	–	8.93	5.28	1.115	8.1	mm
Number of parallel conductors	–	1	–	19	1	–
Effective width of primary core, L_i	0.23	0.216	0.29	0.101	0.1715	m
Pole pitch, τ	0.27	0.2868	0.30	0.25	0.20	m
Length of single end connection, l_e	–	0.3483	–	0.2955	0.3685	m
Coil pitch, w_c	0.225	0.1673	0.25	0.1944	0.1555	m
Airgap, g	15.0	12.6	12.0	15.0	18.2	mm
Number of slots, $z_1(z_1')$	96(106)	72(79)	48(58)	54(61)	36(43)	–
Width of slot, b_{11}	–	15.6	17.0	15.0	13.08	mm
Width of slot opening, b_{14}	–	15.6	–	10.44	13.08	mm
Depth of slot, h_{11}	–	53.0	38.0	34.21	61.47	mm
Height of yoke, h_{1y}	–	43.6	39.3	71.63	50.0	mm
Conductivity of back iron at 20°C, σ_{Fe}	–	4.46	9.52	4.46	5.12	$\times 10^6$ S/m
Conductivity of Al cap at 20°C, σ_{Al}	–	30.0	30.3	32.3	21.5	$\times 10^6$ S/m
Width of back iron, w	0.3	0.24	0.3	0.111	0.1715	m
Thickness of back iron, h_{sec}	19.0	12.5	25.0	25.4	47.4	mm
Thickenss of Al cap, d	5.0	4.5	5.0	4.5(2.5)	3.2	mm
Thickness of Al cap behind Fe core, t_{ov}	5.0	17.0	5.0	12.7	3.2	mm
Width of Al cap, $w + 2w_{ov}$	0.30	0.32	0.40	0.201	0.2985	m

JLMDR = Japanese Linear Motor Driven Railcar, Japan,
ICTS = Intermediate Capacity Transit System, Canada,
KU = Kyushu University LIM, Japan,
CIGGT = Canadian Inst. of Guided Ground Transport, Canada,
GEC = General Electric Company, USA.

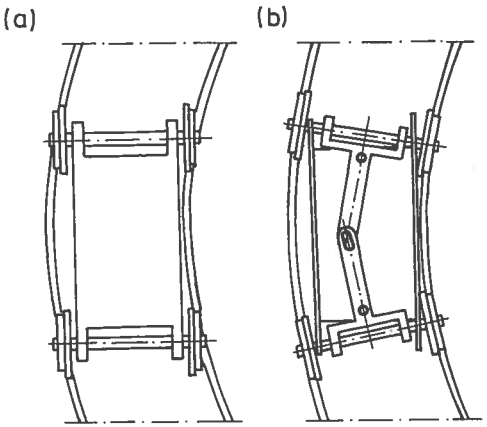

FIG. 1.11. The undercarriage of a wheel-on-rail vehicle: (a) rotary motor propulsion, (b) LIM propulsion.

The congestion problems of big cities should be solved by creating collective transport forms that can be implemented without affecting a highly populated city. For example, there are many cities in Italy where the historical centre has remained the same since the Renaissance. A heavy railway might be a completely wrong solution and have a notable impact on the city planning. An adequate solution might be a light railway, a *people mover*, with transport capacity of 10 to 20 thousand passengers per hour, to replace the traditional transport nets and to integrate the existing railway nets.[117]

All the above requirements can be met by using LIMs as propulsion machines. Replacing electrical rotary motors with linear motors in traction drives (electrical locomotives) generally does not require new tracks, but only their adjustment to linear drives. Single-sided LIMs (Fig. 1.10a, 1.10b) are best, since the normal attractive force of these can strengthen the adhesion of wheels and rails. The airgap is from 10 to 15 mm. Most frequently, the locomotive, car, or cart has two LIMs with short primaries (Fig. 1.10a) assembled in series. The double-layer secondary consists of a solid back iron and an aluminum cap, and is located between the rails. Cables for computer communication with the vehicle and, quite often, collectors for electrical energy delivery to the vehicle are located along the track. Three-phase LIMs are fed from variable-voltage, variable-frequency (VVVF) voltage-source inverters. A linear propulsion system of wheel-on-rail vehicles allows more flexibility (Fig. 1.11), reducing noise on bends and wear of the wheels and rails.

Table 1.4 *Design data of double-sided, three-phase LIMs for propulsion of vehicles*

Quantity	LIM		Unit
	GEC	LIMVR	
Maximum thrust at given below input frequency, F_x	0.85	16.68	kN
Input frequency, f	60.0	173.0	Hz
Input phase current, I_1	200.0	2000.0	A
Number of poles, $2p$	4	10	–
Number of turns per phase, N_1	144	100	–
Diameter of conductor, d_1	0.75	1.10	mm
Effective width of primary core, L_i	0.0869	0.254	m
Pole pitch, τ	0.1795	0.3556	m
Coil pitch, w_c	0.05	0.05	m
Number of slots, $z_1(z_1')$	36(45)	150(160)	–
Width of slot, b_{11}	13.7	16.0	mm
Width of slot opening, b_{14}	13.7	–	mm
Depth of slot, h_1	63.0	–	mm
Height of yoke, h_{1y}	23.9	–	mm
Width of tooth, c_1	20.0	7.7	mm
Resultant airgap, g_t	38.1	38.075	mm
Airgap, g	2×12.7	2×11.1	mm
Thickness of secondary, d	12.7	15.875 (hollow)	mm
Effective thickness of aluminium secondary	12.7	7.2	mm
Width of secondary, w	≥ 0.3046	–	m
Conductivity of aluminium cap at 20^0C, σ_{Al}	≈ 24.34	≈ 24.0	$\times 10^6$ S/m

GEC = General Electric Company, USA,
LIMVR = Linear induction Motor Research Vehicle, Pueblo, Colorado, USA.

Double-sided LIMs (Fig. 1.10c, 1.10d) have found very limited application due to the technical difficulty of eliminating faults caused by bends in the secondary with primary cores on either side. It is more difficult to keep a small and uniform airgap in double-sided LIMs than that in single-sided LIMs.

The *LIM-driven wheel-on-rail vehicles* are built for low velocities, i.e. less than 100 km/h, and for short routes, i.e. less than 50 km (urban transit systems and short-distance trains). At present, LIM-driven trains operate in Toronto and Vancouver, Canada,[30, 140] in Detroit, USA, and Tokyo

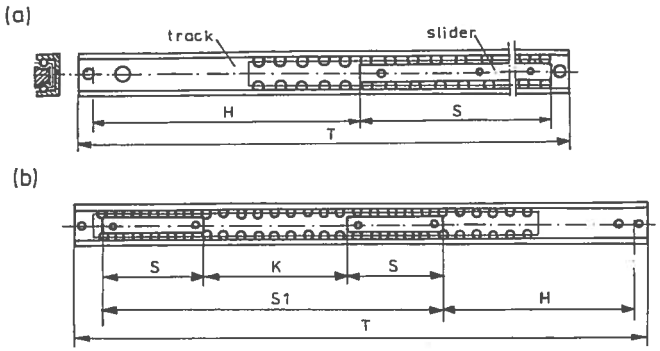

FIG. 1.12. Linear ball bearing with: (a) one slider, (b) two sliders.

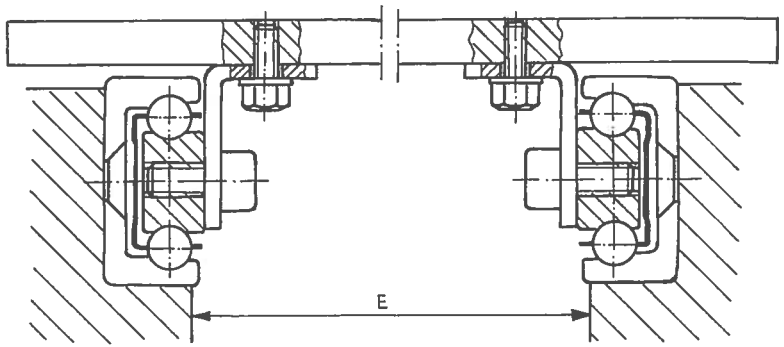

FIG. 1.13. Linear table movement.

and Osaka, Japan.[97, 130] Small car units propelled by LIMs mounted on the track between the rails are used in Walt Disney World (Orlando, Florida) and at Houston Intercontinental Airport (Texas).[65, 136] There have also been attempts to replace steel wheels and rails with air support pads (Dulles International Airport, Washington; Duke University, Durham; UTDC Kingston, Canada).

The design data of some single-sided traction LIMs are presented in Table 1.3 and double-sided traction LIMs in Table 1.4.

1.4 Linear bearings

Linear ball bearings offer a simple solution to reciprocating linear motion problems. A LIM furnished with linear bearings can be used in industrial drives, control systems, and various mechanisms. It includes automation devices, feed mechanisms, packaging machines, sound proofing panels, passenger vehicle doors, welding machines, guides for pneumatic cylinders, X-ray equipment, battery modules, copying machines, etc.

Fig. 1.12 shows a typical linear ball bearing. It consists of a linear bearing track T, slider S, ball cage, and double row of high-precision balls. The slider runs inside a track rail supported by a double row of balls, individually located and spaced by the ball cage.

Fig. 1.13 shows an application involving two linear bearings. It is desirable for the length of the slider S to be very similar to the distance between the track rail E. If the 'wheel-base' S is too small the table top may tend to wobble and jam in the two track rails. It is recommended that ratio $E/S \leq 2$. The two linear bearings must be absolutely parallel. If the table top is very long, linear bearings with two separate short sliders (Fig. 1.12b) should be used.

1.5 Magnetic levitation

High-speed trains need high-precision tracks. The wear time of tracks for high-speed trains is rather short. Therefore, the maximum velocity for traditional railways is 250 to 300 km/h. The world's fastest train TGV Atlantique has established the world rail speed record of 515.3 km/h, but the maximum authorised speed of this train is 300 km/h. At higher speeds, the construction and maintenance of railway systems would not be justifiable from a technical and economical point of view. Nowadays, the transport in highly industrialized countries requires speeds higher than 300 km/h. These requirements can be met by air transport, which, on the other hand, consumes a lot of energy and is expensive. Research done in Germany and Japan shows that vehicles suspended magnetically and propelled by linear motors are the optimum solution to modern transport problems. These magnetic levitation vehicles run at speeds of about 500 km/h on routes longer than 100 km.

Fig. 1.14a shows energy consumption per passenger per 1 km against speed of trains, cars, aircraft, and magnetic levitation trains.[88] The speed of magnetic levitation trains is less than that of airplanes but the energy consumption is much lower. The track costs at high cruising speeds (above 250 km/h) are lower than those for wheel-on-rail trains. Other advantages include low level of noise (Fig. 1.14b), high level of security of riding (Fig. 1.14c), high comfort of riding, easy maintenance, possibility to reach the

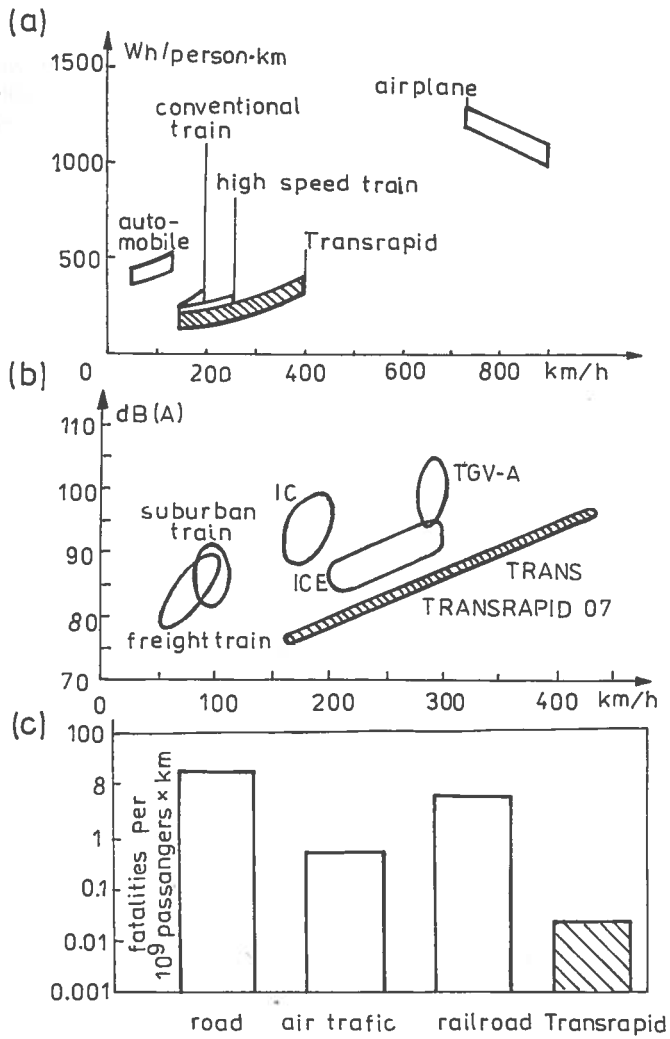

FIG. 1.14. Comparison of passenger transportation systems: (a) energy consumption per passenger per kilometre against speed, (b) maximum noise level at 25-m distance (IC — intercity train, ICE — intercity express, TGV-A — TGV Atlantique), (c) safety analysis — transportation system risk. (Courtesy of Thyssen Henschel, Germany.)

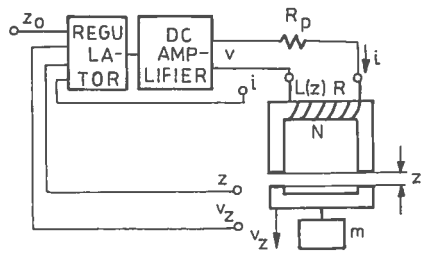

FIG. 1.15. Electromagnetic levitation system: z_o — required airgap, z — actual airgap, v_z — speed of the electromagnet in the z-direction, m — mass of yoke (part being suspended).

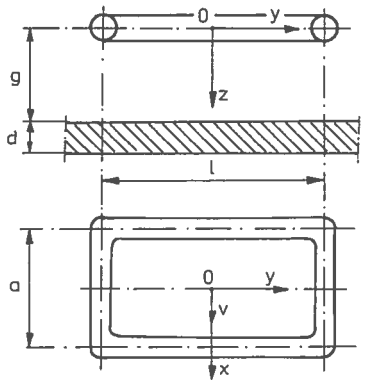

FIG. 1.16. Electrodynamic levitation system: a — coil width, l — coil length, d — aluminium plate thickness, g — airgap.

centres of big cities, low land absorbtion, adaptability to the landscape due to the high gradability of 10% and the short curvature radii of 2.25 km at 300 km/h, and no pollution to natural environment.

Both electromagnetic levitation systems (Fig. 1.15) and electrodynamic levitation systems (Fig. 1.16) are used for the magnetic suspension.

In *electromagnetic levitation systems* the attraction force between the steel yoke (guidance) and electromagnets lifts the vehicle. The electromagnet is fixed to the undercarriage. The current of the electromagnet

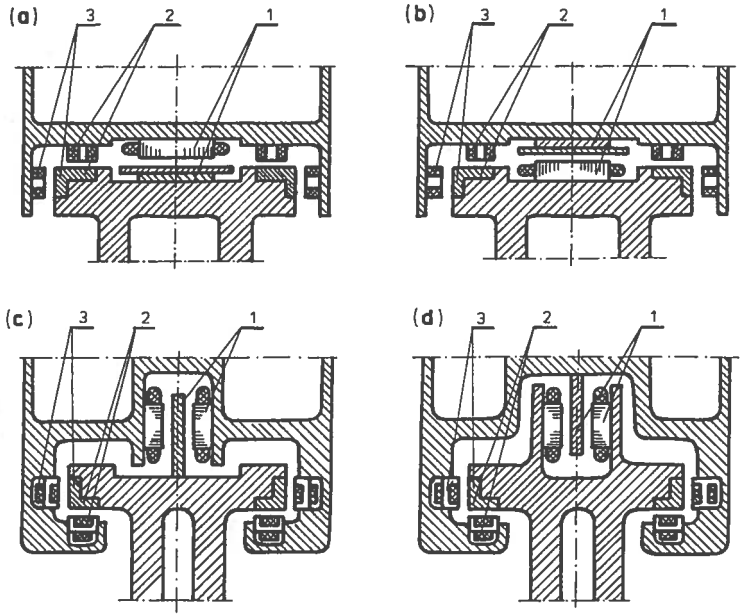

FIG. 1.17. Basic designs of magnetically levitated vehicles propelled by linear motors: 1 — propulsion system, 2 — suspension system, 3 — lateral stabilization system. Description of propulsion systems (a), (b), (c), and (d) is the same as in Fig.1.10.

is automatically controlled. The attraction force can be found using the well-known formula:[36]

$$F_z \approx \frac{\mu_o A_g (Ni)^2}{4g^2} \tag{1.1}$$

where: μ_o is the magnetic permeability of free space, A_g is the area of the airgap under a single pole of the electromagnet, i is the current in the coil of the electromagnet, N is the number of turns of the coil, and g is the airgap.

An electromagnetic levitation system needs a control system. When the airgap between the pole and the yoke increases, the current in the coil of the electromagnet also increases. When the airgap decreases, the current must decrease. In practice, to keep the required airgap z_o constant (about 10 mm), a control system with three feedback signals is used: displacement z, linear velocity v_z in the z direction, and current i.

In *electrodynamic levitation systems* the repulsive forces between the superconductive electromagnet mounted on the undercarriage and an aluminium plate (guidance) fixed to the track are used. The airgap (100 to 300 mm) is much higher than that in electromagnetic levitation systems. Owing to the large airgap, the electrodynamically levitated trains can operate in severe climates with heavy snowfalls, ice formations, and white frost formations. The repulsive force between the d.c. fed coil moving with velocity v and a nonferromagnetic conductive plate placed below the coil can be calculated using Hannakam's [67] formula, which has been modified by Guderjahn *et al*, [64] i.e.

$$F_z = \frac{\mu_o (Ni)^2}{\pi g} \left\{ \sqrt{\left(\frac{l}{2}\right)^2 + g^2} + \sqrt{\left(\frac{a}{2}\right)^2 + g^2} - 2g \right.$$

$$- \left[\sqrt{\left(\frac{l}{2}\right)^2 + \left(\frac{a}{2}\right)^2 + g^2} - \sqrt{\left(\frac{a}{2}\right)^2 + g^2} \right] \frac{g^2}{(a/2)^2 + g^2}$$

$$\left. - \left[\sqrt{\left(\frac{l}{2}\right)^2 + \left(\frac{a}{2}\right)^2 + g^2} - \sqrt{\left(\frac{l}{2}\right)^2 + g^2} \right] \frac{g^2}{(l/2)^2 + g^2} \right\} \frac{1}{1 + k^2} \tag{1.2}$$

where $k = 2/(\mu_o v \sigma d)$ if the plate thickness $d < \delta$ and $k = 2/(\mu_o v \sigma \delta)$ if $d > \delta$. The parameter $\delta = 1/\sqrt{\pi f \mu_o \sigma}$ is the equivalent depth of penetration. The coefficient $1/(1+k^2)$ in eqn (1.2) can also be replaced by $exp\{-\xi/[1 + 2(g/l)^{3/2}]\}$, where $\xi = [4\pi/(\mu_o v \sigma g)]^{1/2}$. The coil moving with velocity v is subject to the braking force $F_x = kF_z$. More detailed discussion of eqn (1.2) is given in Bočarov and Nagorski [9] and Guderjahn *et al.*[64]

A number of details on electrodynamic levitation systems in application to transportation systems can be found in publications by Alscher *et al*,[1] Linacre,[84] Menden *et al*,[88] Miller and Ruoss,[91] Money,[92] Nagaike and Takatsuka,[94] Ohishi, [111] Pascal,[114] Pollard and Riches,[119] Raschbichler and Miller.[121] The basic designs of magnetically levitated vehicles propelled by linear motors are shown in Fig. 1.17.

Table 1.5 shows the most important design data of magnetic levitation vehicles built so far. The projects still in blue print such as the Canadian Maglev System [1] or Russian projects have not been included.

Table 1.5 *Characteristics of magnetic levitation vehicles*

Name of vehicle	Year of introduction	Suspension	Propulsion	Max. speed km/h	Mass of unit t	Load capacity t
Germany						
Transrapid 01	1970	ELM	SLIM	-	-	-
MBB-PV	1971	ELM	DLIM	90.0	5.8	0.6
Transrapid 02	1971	ELM	DLIM	164.0	11.3	0.6
Transrapid 03	1972	AC	DLIM	140.0	10.0	2.0
Transrapid 04	1973	ELM	DLIM	253.0	20.0	1.5
HMB 2	1974	ELM	LSMFe	36.0	2.0	0.3
KOMET	1975	ELM	RM	400.00	9.0	0.2
LSV 301	1975	ELM	LSMFe	20.0	2.2	0.2
EET 01	1974	ELD	DLIM	140.0	17.0	5.0
EET 02	1977	tyred wheels	LSM	230.0	14.0	3.0
Transrapid 05	1979	ELM	LSMFe	75.0	36.0	5.2
Transrapid 06	1983	ELM	LSMFe	400.0	122.0	20.0
M-Bahn	1984	ELM	LSMFe	50.0	7.8	6.0
Transrapid 07	1989	ELM	LSMFe	500.0	100.0	20.0
Japan						
EML-50	1975	ELM	SLIM	40.0	1.8	-
HSST-01	1977	ELM	SLIM	307.8	1.0	-
HSST-02	1977	ELM	SLIM	110.0	1.8	0.6
HSST-03	1985	ELM	SLIM	60.0	12.3	5.7
HSST-04	1987	ELM	SLIM	43.0	19.8	7.2
HSST-05	1988	ELM	SLIM	55.0	39.5	14.5
ML-500	1977	ELD	LSM	517.0	10.0	1.5
MLU001	1980	ELD	LSM	400.0	10.0	1.5
Rumania						
Magnibus 01	1984	ELM	HLSM	54.0	3.0	-
UK						
BMS	1984	ELM	SLIM	42.0	8.0	3.2

AC = air cushion,
BMS = Birmingham Maglev System,
DLIM = double-sided LIM,
ELM = electromagnetic levitation, ELD = electrodynamic levitation,
HLSM = homopolar linear synchronous motor,
LSM = air-core linear synchronous motor,
LSMFe = linear synchronous motor with ferromagnetic core,
RM = rocket motor,
SLIM = single-sided LIM.

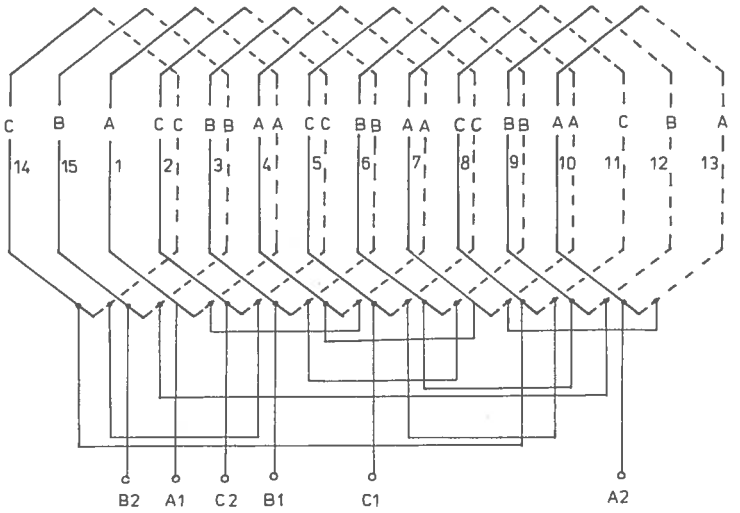

FIG. 1.18. Three-phase, double-layer winding of a small, flat LIM with $2p = 4$, $q_1 = 1$, and with six half-filled end slots.

1.6 Windings

The *primary windings* of LIMs are copper conductors with round or rectangular cross-section. Aluminium conductors are not used since they increase the primary winding losses and, consequently, the winding temperature. The windings can be located in slots, i.e. windings with *distributed parameters* or in the form of coils located on salient poles (in flat LIMs with transverse flux or in some tubular LIMs), i.e. windings with *concentrated parameters*. Low-power LIMs have *random windings* made from round wire (semi-open slots), while medium-power and large LIMs have *windings made from preformed coils* from rectangular copper bars (open slots). The insulation class is usually F or H. The current density in the primary windings is from 4 to 25 A/mm^2 and depends on the output power and on the cooling system. When the primary current density is more than 15 A/mm^2, the conductors have *internal channels* and *direct water cooling* system is required.

The primary windings are usually three-phase windings with the number of slots per pole per phase $q_1 = z_1/(2pm_1) > 1$, where z_1 is the number of primary slots totally filled with conductors, m_1 is the number of primary phases, and $2p$ is the number of primary poles. The larger is q_1, the closer is the distribution of magnetic flux density along the x axis to

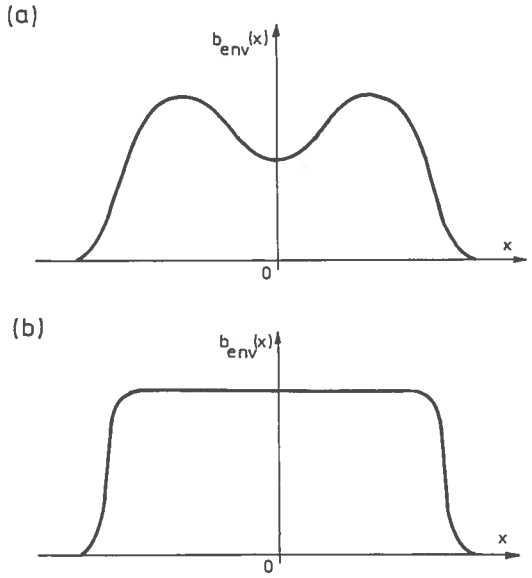

FIG. 1.19. The envelope b_{env} of the space–time distribution along the x axis of the normal component of the airgap magnetic flux density produced by a three-phase, double-layer, four-pole winding: (a) without compensating coils, (b) with compensating coils.

a sinusoidal function. This rule is not applied to low-power LIMs with small dimensions. For these LIMs, $q_1 = 1$. To improve the distribution of the magnetic flux density and reduce the resistance and leakage reactance, chorded windings are quite common. Therefore, it is better to design flat LIMs with *double-layer primary windings* than LIMs with *single-layer windings*.

It is very important to obtain small resistance and leakage reactance of the primary windings of LIMs with large airgaps. The airgap of single-sided LIMs is from a few to several millimetres, and the nonferromagnetic airgap of double-sided LIMs is much larger, i.e. it can reach a few centimetres. The large magnetizing current magnifies the input current, which in turn results in much higher voltage drops in the primary circuit than in the case of rotary induction motors where the airgap is from a fraction of a millimetre to a few millimetres.

A double-layer winding fills only half of the slots at each end of the core, i.e. the end slots accommodate only one side of a coil, which causes

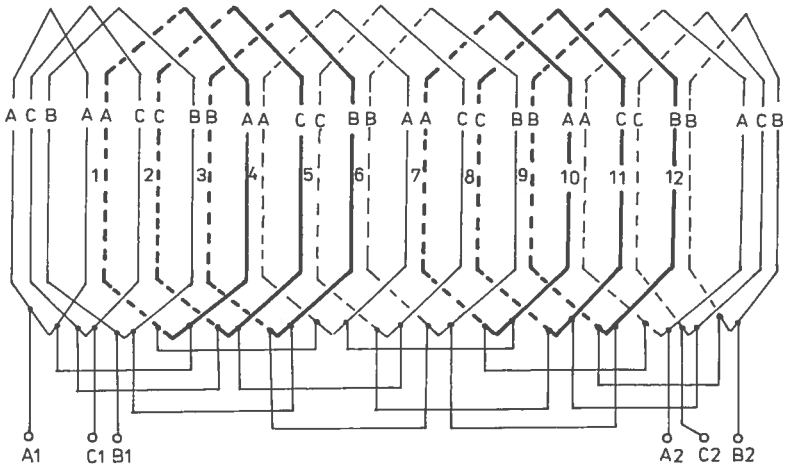

FIG. 1.20. Three-phase, double-layer winding of a small, flat LIM with $2p = 4$, $q_1 = 1$, and with compensating coils. The thin line shows the coils containing one-third of the number of slot conductors. The solid line shows the coils containing two-thirds of the number of slot conductors.

nonuniform distribution of MMF along the x axis, weakened at each end of the primary core. Owing to this fact and to the necessity of compensating the pulsating component of magnetic flux density, so-called *compensating coils* are applied.[139] The pulsating component of magnetic flux density is caused by the *end effects*. The additional compensating coils create supplementary groups of coils and are located in the half-filled end slots. Fig. 1.18 shows a double-layer winding with $m_1 = 3$, $2p = 4$, $Q_1 = 3$, and

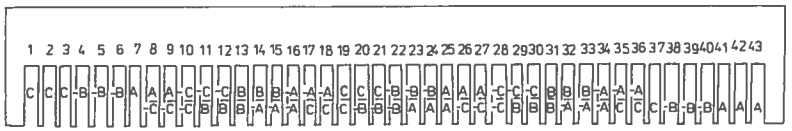

FIG. 1.21. Three-phase, double-layer winding of a large, flat LIM with $2p = 4$, $Q_1 = 9$, $q_1 = 3$, and $w_c/\tau = 7/9$, without compensating coils.

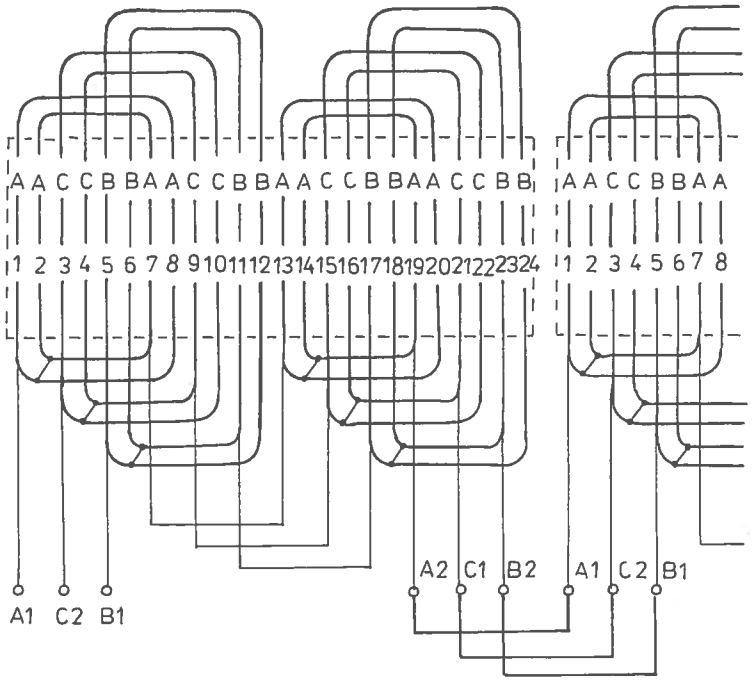

FIG. 1.22. A single section of a three-phase, single-layer winding with $2p = 4$, and $q_1 = 2$ of a flat LIM with segmented primary core.

$q_1 = 1$ of a small LIM. There are three half-filled slots at each end of the primary core. The number of slots $z_1 = 12$ assumed for calculations is equal to the number of slots totally filled with conductors, i.e. nine plus 50% of half-filled slots, i.e. $9 + 0.5 \times 6 = 12$. The total number of slots for such a winding is

$$z_1' = \left(2p + \frac{w_c}{\tau}\right) m_1 q_1 = \frac{1}{2p}\left(2p + \frac{w_c}{\tau}\right) z_1 \tag{1.3}$$

The envelope b_{env} of the space–time distribution $b(x,t)$ of the magnetic flux density in the airgap of a LIM with the primary winding according to Fig. 1.18 is shown in Fig. 1.19a (the influence of slotting is neglected). Unfavourable distribution of the magnetic flux density along the x coordinate, weakened at each end of the core, can be seen. After adding the compensating coils, the winding diagram becomes more complicated (Fig.

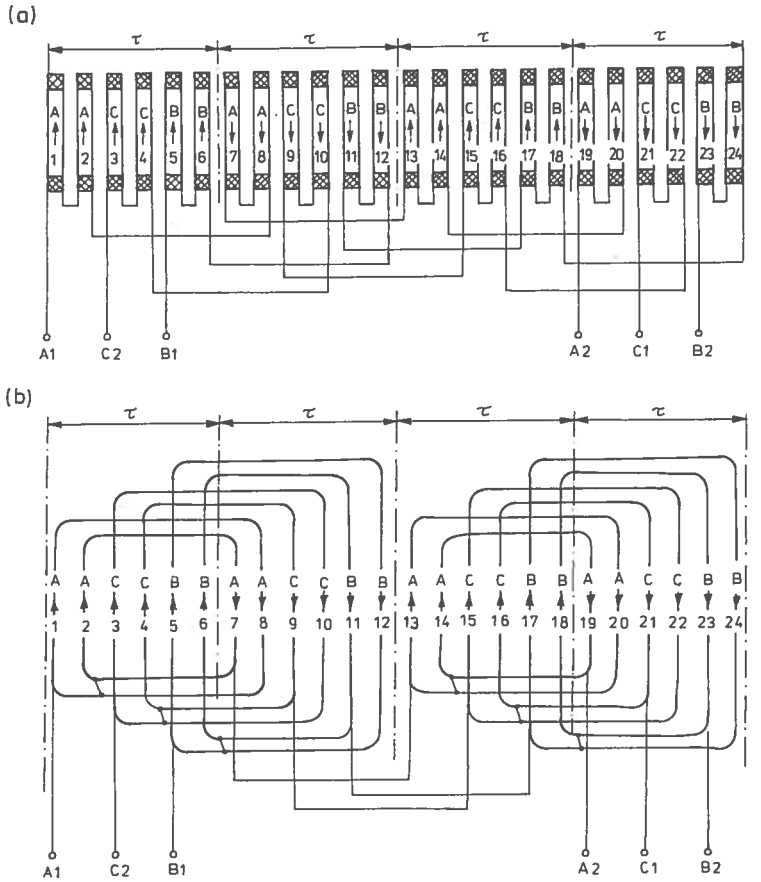

FIG. 1.23. A single-layer winding of three-phase LIMs with $2p = 4$, $z_1 = 24$, and $q_1 = 2$: (a) tubular LIM, (b) flat LIM.

1.20) but the envelope of the magnetic flux density (Fig. 1.19b) — neglecting the slotting — is parallel to the x axis within the interval $0 \le x \le 2p\tau$. When calculating the reactances, the equivalent number of turns per phase for the windings with compensating coils, as shown in Fig. 1.20, can be assumed

$$N_1' \approx N_1 + \frac{w_c'}{w_c} N_{1c} \tag{1.4}$$

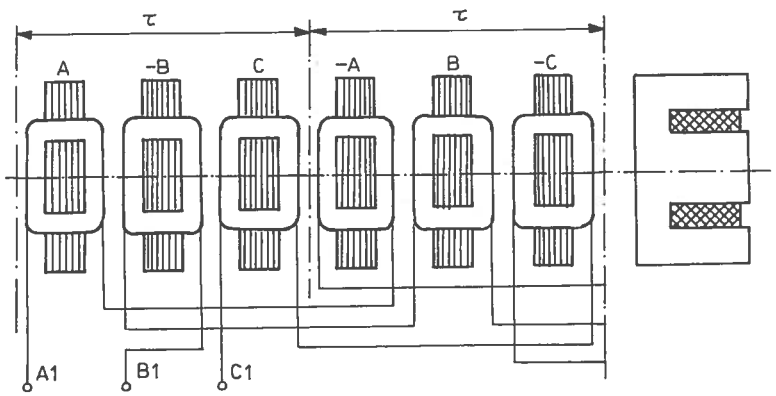

FIG. 1.24. Connection diagram of coils of a three-phase, single-sided LIM with transverse magnetic flux.

where N_1 is the number of turns per phase, N_{1c} is the number of compensating turns per phase, w_c is the coil pitch, and w_c' is the compensating coil pitch. The typical ratio $w_c'/w_c \approx 1/3$ for small single-sided LIMs.[99] The compensating coils are applied only to small LIMs with $2p \leq 4$. In medium-power and large LIMs with $2p > 4$, the compensating coils are not necessary since the ratio *number of half-filled slots to total number of slots* is small (less than or equal to 0.2). Fig. 1.21 shows a three-phase, double-layer winding of a large LIM with $2p = 4$, $Q_1 = 9$, $q_1 = 3$, and $w_c/\tau = 7/9$, without compensating coils.

Single-layer windings should be used either for flat LIMs with *segmented primary core*, e.g. for traction LIMs with long primary fixed to the track, or for tubular LIMs. A single-layer winding of a flat LIM with segmented primary core is shown in Fig. 1.22. A single-layer winding of a tubular LIM (Fig. 1.23) consists of *cylindrical coils* and is created by rolling the flat winding (Fig. 1.23b) around the x axis (Fig. 1.3). The beginnings and the ends of the conductors are connected together so that the end connections are eliminated. This is the fundamental advantage of tubular motors. The windings of tubular LIMs can also be equipped with compensating coils.[139]

The windings of LIMs with transverse magnetic flux (Fig. 1.24) consist of coils with concentrated parameters and rectangular cross-section, and are made similarly to windings of small transformers. If the phase sequence is A,-B,C,-A, B,-C,..., the shape of the MMF wave will be close to the sinusoidal, which means the LIM will produce the highest thrust. The same phase sequence can also be used in tubular motors.

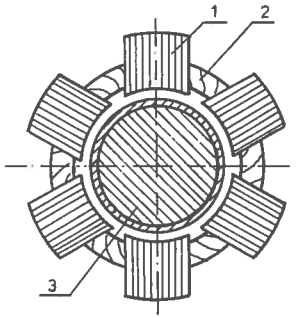

FIG. 1.25. Laminated core of a tubular, single-sided LIM consisting of six segments: 1 — single segment, 2 — primary winding, 3 — double-layer secondary.

The *secondary windings*, in general, have distributed parameters. In single-sided LIMs (Fig. 1.3a) the secondary winding consists of a solid steel core (back iron), whose surface adjacent to the airgap is covered with *aluminium* or *copper layer*. Laminated secondary cores are rather rare. The thickness of the aluminium layer is from 2 to 6 mm, while the thickness of the copper layer is from 1 to 4 mm. In general, flat LIMs (Fig. 1. 3a) have an aluminium cap and single-sided tubular LIMs (Fig. 1.5a) have a copper cap. A solid secondary core is a conductor both for magnetic flux and for electric current.

The secondary of double-sided LIMs usually does not have a ferromagnetic core. In flat, double-sided LIMs the secondary is an *aluminium* or *copper plate* (Fig. 1.3b) and in double-sided tubular LIMs (Fig. 1.5c) the secondary is *aluminium* or *copper pipe*. The thickness of a copper or aluminium secondary ranges from a few to several millimetres. In many cases a nonferromagnetic secondary of flat, double-sided LIMs is hollow or it consists of two aluminium layers with an insulating nonferromagnetic layer between them, e.g. air.

Secondary *cage (ladder) windings* or phase windings are rather rare. Their construction is similar to the rotor windings of rotary induction motors (Section 4.3).

1.7 Magnetic circuits

Magnetic circuits of LIMs are made of the same magnetically soft materials as those of rotary machines, i.e. they are made from *nonoriented, cold-rolled electrotechnical steel sheets*. The thickness of the sheets is 0.2 – 0.65 mm and the silicon content is 0.3 – 3.2% or sometimes no silicon is added. In

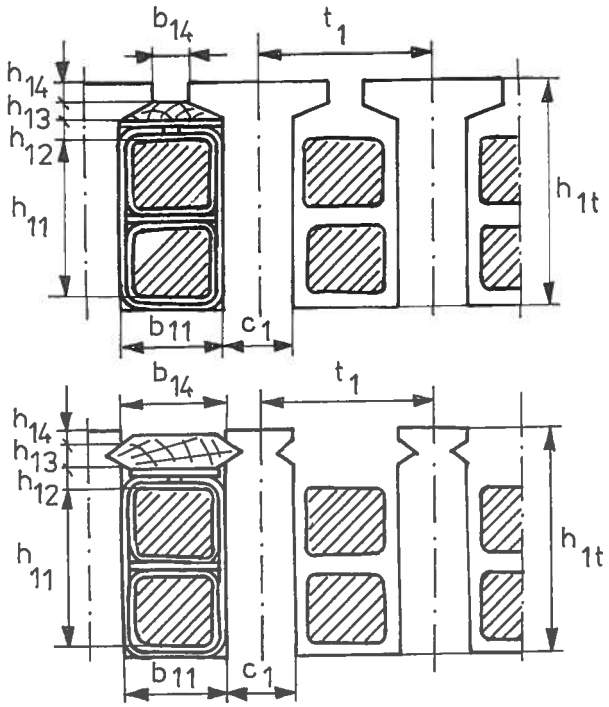

FIG. 1.26. The primary slots of flat LIMs: (a) semi-open, (b) open.

low-speed LIMs fed from a $5-10$ Hz power source, it is possible to replace electrotechnical steel sheets with steel sheets of thickness up to 2.5 mm used for deep drawing (lower wear of punch and die). It is better to produce the primary cores of tubular motors, due to their complicated shapes, by powder metallurgy (*sintered ferromagnetic powders*).[76] A simple primary core of a tubular LIM made of electrotechnical steel sheets (Fig. 1.25) consists of from four to eight rectangular segments located uniformly around the periphery. In large LIMs with transverse flux, the primary cores of which are almost the same as transformer cores, oriented (anisotropic) steel sheets can be used.

The thickness of the edge sheets of laminated cores is increased to about 1.5 mm. Instead of applying thick edge laminations it is better to weld together a couple of normal thickness edge laminations since punch and die are not designed to cut thick sheets. To improve the heat transfer, it is recommended that cooling ducts be perpendicular to the conductors in

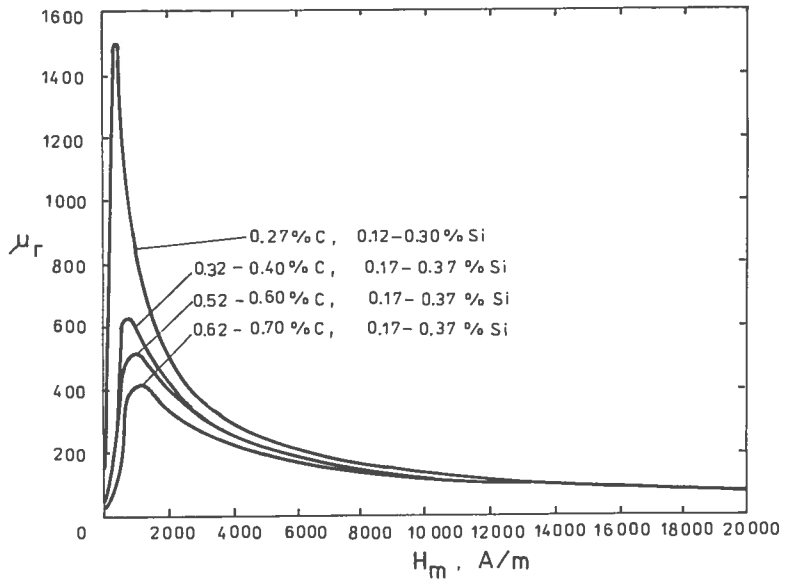

FIG. 1.27. Magnetization curves $\mu_r(H_m)$ of carbon steels.

large LIMs. The recommended width of cooling ducts is $6-15$ mm, about 10 mm on average.

Traction LIMs with large pole pitches $\tau = 200 \ldots 300$ mm and number of poles $2p > 6$ have a primary core of at least 1.2 m length. It is wise in these motors to divide the laminations into shorter segments and then to assemble them in such way that the segments in each alternate layer are shifted by half the segment length.

The primary slots (Fig. 1.26) of flat LIMs are rectangular and are semi-open (for random windings) or open (for preformed coils).

The secondary cores of flat and tubular LIMs are hardly ever laminated or sintered. In general, there are *solid cores* made from flat steel bars or plates (flat LIMs), or from round steel bars or pipes (tubular LIMs). The thickness of solid cores is usually from 10 to 30 mm at input frequency 50 or 60 Hz. The radius of the secondary core of a tubular LIM should also be from 10 to 30 mm. The less thick the core, the lower is the thrust and the power factor due to an increase in the magnetizing current (increased magnetic voltage drop in the secondary core.)[53] On the other hand, the thick secondary ferromagnetic core enlarges the dimensions and the costs of a linear drive. In practice, the thickness does not exceed 25 mm.

Fig. 1.27 shows the magnetization curves $\mu_r = f(H_m)$, where μ_r is the relative magnetic permeability, of typical carbon steels which can be used for manufacturing the secondary cores of LIMs. The electrical conductivities of those steels are from 4.5×10^6 to 6.2×10^6 S/m.[32]

The *saturation factor of the magnetic circuit* for LIMs is defined similarly to that for rotary induction motors, i.e.

$$k_{sat} = 1 + \frac{2V_{\mu 1t} + 2V_{\mu 2t} + V_{\mu 1y} + V_{\mu 2y}}{2V_{\mu gt}} \tag{1.5}$$

where: $V_{\mu 1t}$ is the magnetic voltage drop across the primary single tooth, $V_{\mu 2t}$ is the magnetic voltage drop across the secondary single tooth, $V_{\mu 1y}$ is the magnetic voltage drop of the primary yoke, $V_{\mu 2y}$ is the magnetic voltage drop of the secondary yoke, and $V_{\mu gt}$ is the magnetic voltage drop across the total (resultant) airgap g_t multiplied by Carter's coefficient. For LIMs with a solid secondary, $V_{\mu 2t} = 0$ (no teeth).

The total airgap is:

- for single-sided LIMs (Fig. 1.3a, 1.5a, 1.5b)

$$g_t = g + d \tag{1.6}$$

- for double-sided LIMs (Fig. 1.3b, 1.5c)

$$g_t = g_1 + g_2 + d \tag{1.7}$$

where: d is the thickness of the high-conductivity layer and g, g_1, and g_2 are the mechanical clearances.

Some researchers, e.g. Voldek [139] use the *saturation factor of the teeth*

$$k_{satt} = 1 + \frac{2V_{\mu 1t} + 2V_{\mu 2t}}{2V_{\mu gt}} \tag{1.8}$$

and the *saturation factor of the yokes*

$$k_{saty} = 1 + \frac{V_{\mu 1y} + V_{\mu 2y}}{2V_{\mu gt} + 2V_{\mu 1t} + 2V_{\mu 2t}} \tag{1.9}$$

The resultant saturation factor is then

$$k_{sat} = k_{satt} k_{saty} \tag{1.10}$$

Since the *saturation magnetic flux density* for cold-rolled electrotechnical steel sheets is about 0.5 T higher than that for carbon mild steels, the magnetic permeability of laminated cores is much higher than the permeability of solid cores. Therefore, for LIMs containing solid secondary cores, particularly under high magnetic saturation, the following inequality is valid:

$$2V_{\mu 1t} + V_{\mu 1y} \ll 2V_{\mu 2t} + V_{\mu 2y} \tag{1.11}$$

and the saturation factor of the magnetic circuit can be expressed using a simplified formula

$$k_{sat} \approx 1 + \frac{2V_{\mu 2t} + V_{\mu 2y}}{2V_{\mu gt}} \tag{1.12}$$

The calculation of the magnetic voltage drop of a solid ferromagnetic core is made on the basis of the distribution of the magnetic field intensity. There is always some calculation error. The longer the pole pitch, the higher the calculation error. The calculation results of $V_{\mu 2y}$ should be regarded as simplified, particularly for LIMs with long pole pitches (traction LIMs), i.e. $\tau \geq L_i$.

Carter's coefficent k_C of the airgap should be calculated using the exact formula. According to Carter, for the primary core:[68]

$$k_{C1} = \frac{t_1}{t_1 - \gamma_1 g_t} \tag{1.13}$$

where

$$\gamma_1 = \frac{4}{\pi}\left\{\frac{b_{14}}{2g_t}\arctan\frac{b_{14}}{2g_t} - \ln\sqrt{\left[1 + \left(\frac{b_{14}}{2g_t}\right)^2\right]}\right\} \tag{1.14}$$

where t_1 is the primary slot pitch and b_{14} is the primary slot opening. For large LIMs $b_{14} < g_t$ or $b_{14} \approx g_t$. The approximate formulae in which $b_{14}/g_t > 1$ results in errors in the calculations.

The Carter's coefficient k_{C2} for a slotted secondary core can also be calculated with the aid of eqns (1.13) and (1.14), putting t_2, γ_2, and b_{24} instead of t_1, γ_1, and b_{14}, respectively. The resultant Carter's coefficient is

$$k_C = k_{C1} \times k_{C2} \tag{1.15}$$

For *single-sided LIMs with an aluminium cap* it is recommended to use the following modified Carter's coefficient

$$k_{Cg} = \frac{k_C(g + d)g + d^2 - gd}{g^2 + d^2} \tag{1.16}$$

to obtain an effective airgap $k_{Cg}g$, instead of $k_C g$.

for example, Dombrovsky and Khutorietsky [23] and Richter.[124, 125] The remaining symbols are: m_1 = number of phases, h_{1t} = height of the primary tooth, h_{1y} = height of the primary yoke, b_{11} = width of the primary slot, d = thickness of the high-conductivity layer, L_i = effective width of the primary stack, t_{ov} = thickness of the high-conductivity layer behind the back iron, w = width of the secondary core (back iron), w_{ov} = width of the secondary 'side bars', J_1 = primary current density, and k_i = stacking factor of the primary core.

Assuming the coefficients γ_1, γ_{1Fe}, γ_{2Al}, and γ_{2Fe} are equal to unity, the functions F_1 and F_2 express the volumes of the active materials. If these coefficients are equal to specific mass densities, the functions F_1 and F_2 express the masses of the active materials. If these coefficients are equal to the costs per volume, the functions F_1 and F_2 express the costs of the active materials.

The basic constrains imposed on LIM design are: (1) minimum value of the product $\eta \cos\phi$, (2) maximum magnetic flux densities in any ferromagnetic portion of the magnetic circuit, (3) maximum temperature of the primary winding, (4) maximum length L_τ of the primary core, and (5) maximum value of the space factor of the primary slots. Additionally, for inverter-fed LIMs, (6) maximum permissible peak value of the pulsating thrust, (7) maximum commutation time, and (8) maximum permissible voltage across the terminals of the commutation capacitors of the inverter. The LIM and the inverter should be designed simultaneously.

The extremum of the objective function $F(\overline{x})$ of several variables can be obtained by the first-derivative test (equating the partial derivatives to zero), using gradient methods, nonlinear programming, dynamic programming, and other methods.

The quality of the designed LIM can be evaluated with the aid of the *goodness factor*

$$k_Q = \frac{I_2'}{I_\Phi} = \frac{X_g}{|\,\mathbf{Z}_2'(s)\,|}s \tag{8.98}$$

where I_2' is the secondary current referred to the primary system, I_Φ is the magnetizing current, X_g is the mutual reactance, $\mathbf{Z}_2'(s)$ is the secondary impedance, and s is the slip for the fundamental harmonic. The higher the goodness factor k_Q at a given slip, the better the LIM.

9

EXPERIMENTAL TESTS

Experimental tests play a very important part in the research and design of linear electric drives. Since errors in calculation are always possible, the parameters must often be indentified on physical models in order to verify the accuracy of calculations. A digital simulation of an electromechanical system also requires knowledge of its parameters which should when possible, be measured on the same or similar real system. The successful design of a new linear drive is nearly always accompanied by prior experimental tests performed on a physical model.

9.1 Test facilities

The majority of applications of LIMs, e.g. electrical traction or industrial drives, demand full knowledge of their characteristics during motoring, braking and generating modes. To obtain the steady-state velocity and required accuracy of measurements, the test facilities incorporate a long secondary and are designed according to one of the following options:

(a) a short primary installed in a car riding on a linear track;[118]

(b) a short primary installed in a car which is fixed to an arm and is riding on a circular track;[16, 17, 93]

(c) a motionless, short, double-sided primary propelling an elastic conductive closed belt, similar to a conveyor belt;[37]

(d) a motionless short primary propelling a cylinder, drum, or disc.[21, 39, 107, 122]

All of the above-mentioned facilities are aimed at testing flat LIMs. Tubular LIMs can be tested using facility (a).

A few metres to several hundred metres (depending upon the synchronous velocity) of linear track with a flat LIM mounted to the undercarriage of a wheel-on-rail car is very expensive to test and requires installation in a large assembly house or secure open-air space. In research laboratories, such an option is economically justifiable only for testing small LIMs. When a linear track is not long enough to achieve steady-state velocity, the steady-state characteristics of the LIM being tested can be determined on the basis of dynamic tests.[118]

The circular track test facility built at the University of Palermo, Italy, uses a flat, single-sided LIM riding around a double-layer, aluminium-capped reaction rail which lies in the horizontal plane.[16, 17] The mean diameter of the reaction rail is 9.6 m and its width is 0.9 m. The short primary is mounted on one end of an arm, spinning around a vertical shaft. A counterweight fixed to the other end of the arm balances the centrifugal forces. In addition, the LIM and the counterweight are supported by four idle wheels which are allowed to move along two circular guide rails. The electric energy delivered to the primary unit is provided through three sliding contacts. An additional external 10.6-m diameter circular secondary for a double-sided LIM, replacing the counterweight, has been built recently. In this way, load tests on both the single-sided and double-sided LIM, can be performed for each LIM operating either as a motor or as a brake. The layout of the test facility employing both the single-sided and double-sided LIMs is shown in Fig. 9.1, while the LIMs are shown in Fig. 9.2.

The test facility with a closed belt secondary (Fig. 4.14) poses a serious problem when manufacturing a durable and flexible nonferromagnetic current conducting belt.[37, 120] Usually, it is impossible to make a homogeneous belt.

The simplest, most durable, and most reliable test facilities are those where a motionless primary propels a wheel, drum, or disc. Testing the LIM in motoring, generating, and braking modes is easy. The LIM can easily be loaded using a rotary machine. The measurements of forces and velocity are simple. The thrust F_x and linear velocity can be measured in the same way as the shaft torque and shaft speed of rotary motors. The layout of components is shown in Fig. 9.3a, while the electrical power circuit is shown in Fig. 9.3b. The LIM in Fig. 9.3 is composed of an arc-shaped primary unit and a cylindrical rotor (secondary unit). The motionless primary unit is mounted in such a way as to assure its three-degrees of freedom. Three-directional displacement enables the measuring of thrust, normal force, and lateral force with the aid of loads cells. The cylindrical rotor shaft is coupled with a d.c. machine which can function as a motor, generator, or brake. Both static and dynamic tests can be carried out. The largest test facility of this type has been built at the INREST laboratory in Grenoble, France. The 12-m diameter rotating wheel with horizontal axis is installed in a special bunker.[26, 120] The second largest test facility, with 7.6-m diameter rotating wheel with vertical shaft, has been built at Queen's University (CIGGT), Kingston, Canada. The Kyushu University, Fukuoka, Japan, test facility has a 1.4-m rotating wheel with a horizontal axis.[107] A test facility [39] with a disc-type secondary and a flat primary is shown in Fig. 9.4. Using a flat primary and a rotating disc, the parasitical braking forces due to the disc curvature contribute to errors in the thrust

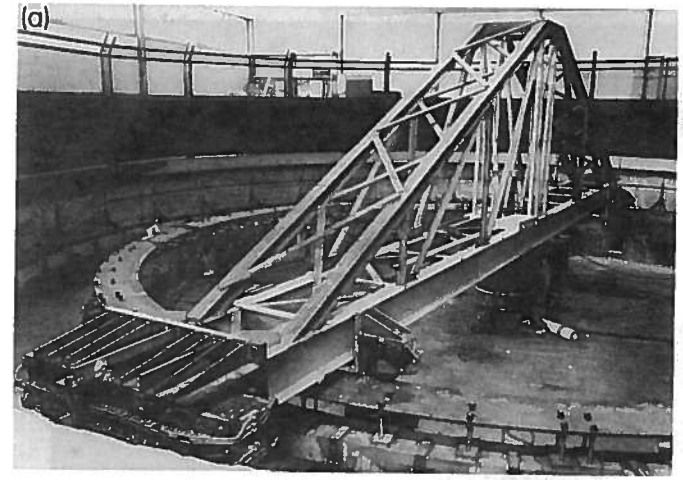

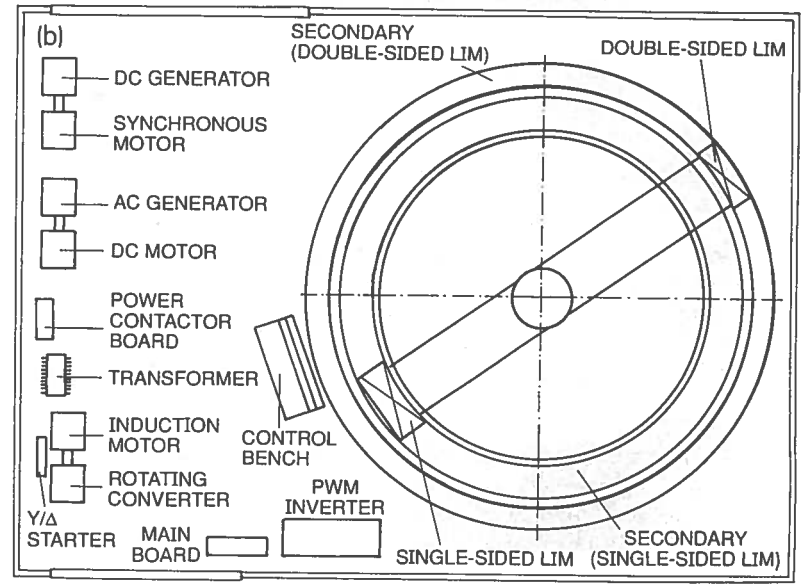

FIG. 9.1. Test facility built at the University of Palermo, Italy: (a) general view, (b) layout. (Photo courtesy of Prof. Cecconi and Prof. Di Maio.)

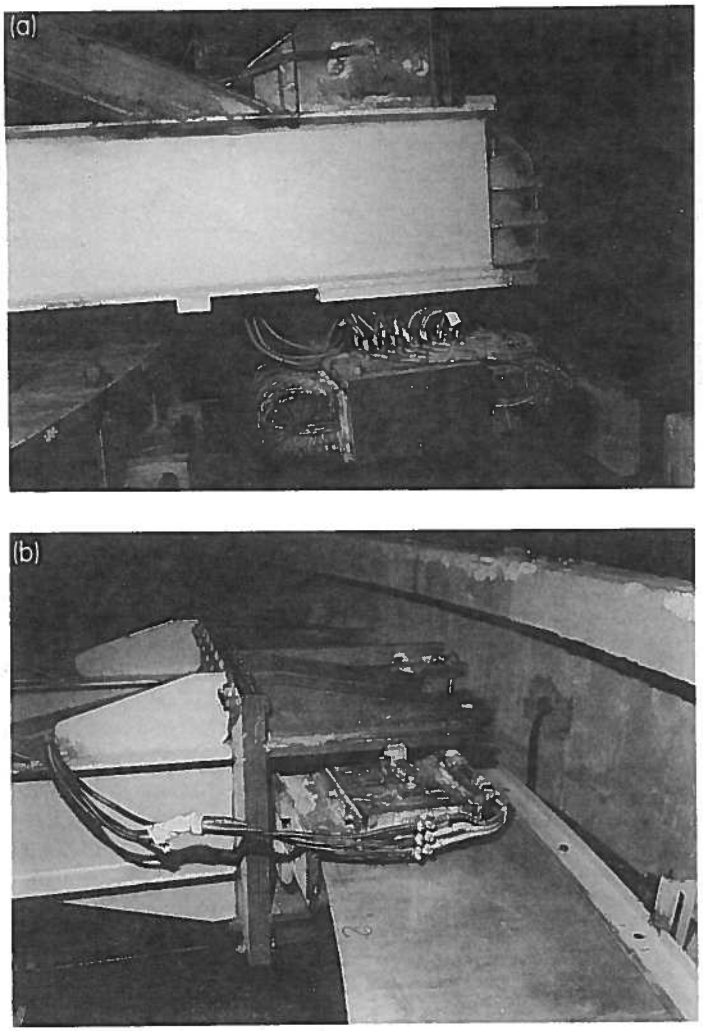

FIG. 9.2. Components of the test facility buil at the University of Palermo, Italy: (a) single sided LIM, (b) double-sided LIM. (Photo courtesy of Prof. Cecconi and Prof. Di Maio.)

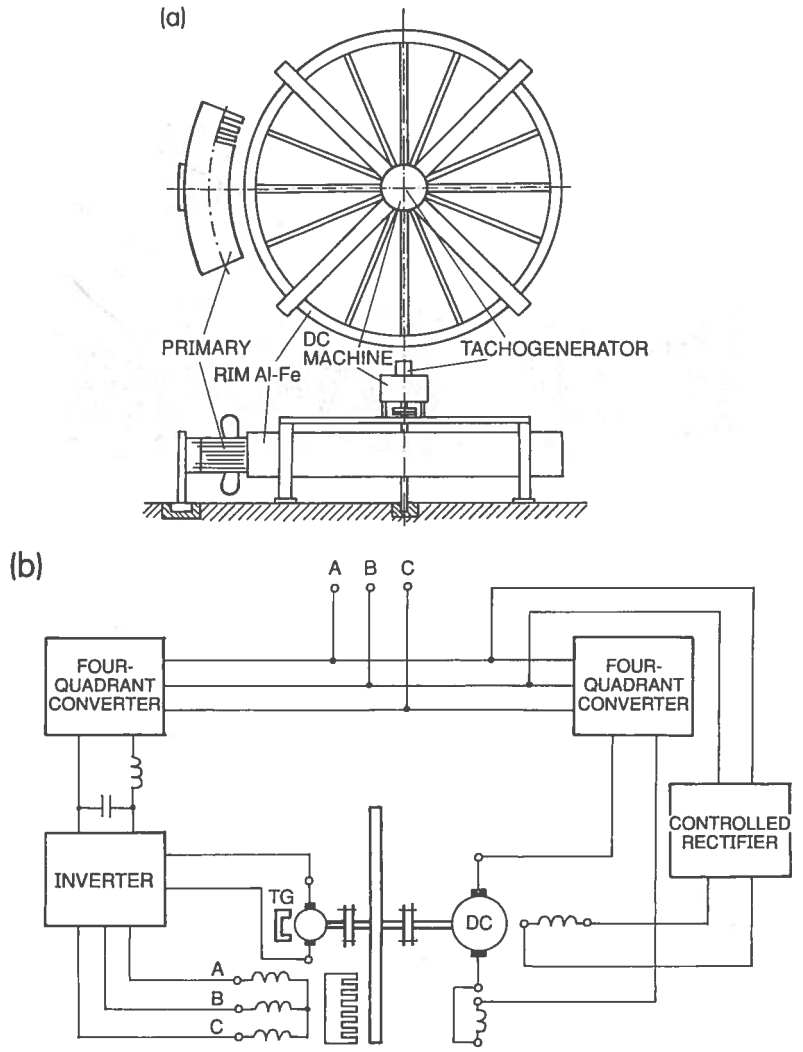

FIG. 9.3. Test facilty consisting of a short primary and a large diameter cylindrical secondary: (a) layout, (b) power electric circuit.

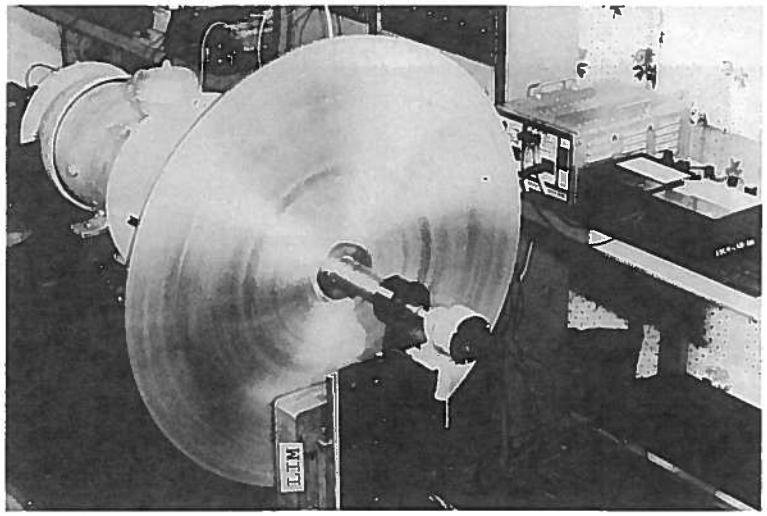

FIG. 9.4. Facility with a disc-type secondary for testing small LIMs built by the author.

measurements. These errors should be estimated and the measurements corrected.

9.2 Data acquisition system

The object of any data acquisition and processing system is to collect the data, and then process it in the desired fashion, record the results in a form suitable for storage, presentation, or additional subsequent processing, control the measurements with high timing accuracy or exact synchronization requirements, and improve the quality of measurement. Such tasks cannot be solved manually or at least can only be solved inadequately.

Tasks that could be performed only by mainframe or minicomputers a few years ago, can now be performed by PCs. A *PC-based data acquisition system* for testing LIMs is sketched schematically in Fig. 9.5. The *interface* converts the data from its present form into another. *Transducers* convert either nonelectrical quantities, i.e. stimulus (position, acceleration, force, temperature, light) into an electrical signal, or an electrical signal into another with different parameters. The transducer produces an output voltage which is amplified to become compatible with the input voltage of the *analog-to-digital* (A/D) *converter*. The A/D converter converts an analog voltage to a digital value. Then, two continuous data domains, for

instance voltage and time, are digitized. How precisely an A/D converter can perform the data conversion is described by the precision, linearity, frequency response, and hysteresis of the transducer plus sampling rate, resolution, and throughput. *Sampling rate* is the number of A/D conversions performed per second. *Resolution* or *dynamic range*, dictates how many discrete values (number of bits) can be assigned to the analog level. *Throughput* or acquisition rate is the amount of data (number of samples per second) collected during a specific amount of time. The *digital-to-analog* (D/A) *converter* outputs an analog voltage for a specific digital value. The analog signals generated by a D/A converter are normally used to control a device. The voltage sent to the device, e.g. static converter, causes the device to operate at a specific rate. Power bipolar transistors, MOSFETs, and IGBTs require a wide range of supply voltage. *Isolation devices* must be capable of relaying the fast switching signals to the device in electrically noisy environments. The *optocouplers* allow for safe, easy interfacing between the control circuit and the power circuit of drive.

There are hundreds of interface cards with A/D and D/A converters available for IBM compatible PCs. For example, the PC-30B features 16 analog input channels with 30 kHz throughput, two 12 bit D/A outputs,

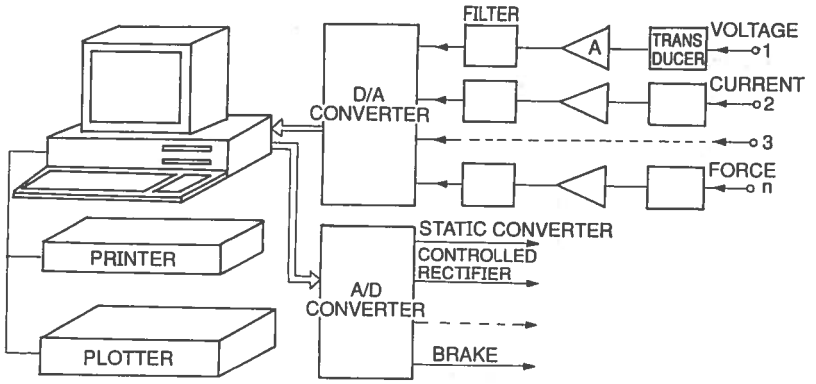

FIG. 9.5. PC-based data acquisition system for testing LIMs.

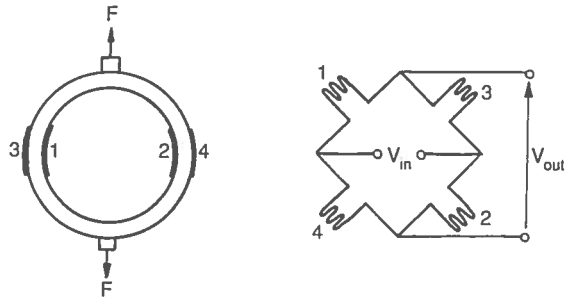

FIG. 9.6. Bonded strain gauge force transducer (load cell).

two 8 bit D/A outputs and 24 digital I/O lines. Most of the interface manufacturers provide some software to get the user started and ensure that the hardware is operating correctly. Normally, a data acquisition system created for the specific purpose requires the development of a software.

9.3 Measurement of forces

The thrust, normal, and lateral forces are, in general, measured using load cells. A *load cell* is a bonded strain gauge force transducer (Fig. 9.6). The circuit commonly used is some form of d.c. Wheatstone bridge. Since the variations in strain are dynamic the bridge circuit is operated in the unbalanced condition, e.g. an output proportional to the variation in the resistance of the active gauge is obtained. To increase the sensivity, two or four active gauges may be used. Load cells measure mass and force from a few grams to a few hundred kilograms (a few thousand Newtons) with a high degree of accuracy and almost no deflection. Accuracy ranging from 0.2% up to 0.03% is standard. It is easily to install the loadcells in test facilities having a motionless primary unit and rotating secondary. The primary must have three degrees of freedom, which allow its diplacement in three axes and measurement of the forces in three directions. The flexible support can be provided with the aid of linear bearings or rollers. The arc-shaped primary unit should be able to rotate freely about the central axis of the test facility. The load cells are installed between the movable and immovable part of the frame to detect the forces between them. Usually, a minimum of two load cells per direction are installed. The Kyushu University test facility [107] uses two load cells for thrust, four compression load cells for normal force, and two compression load cells for the vertical force measurements. A sketch of the location of the load cells is given in Fig. 9.7. The forces are converted into d.c. voltages through strain amplifiers.

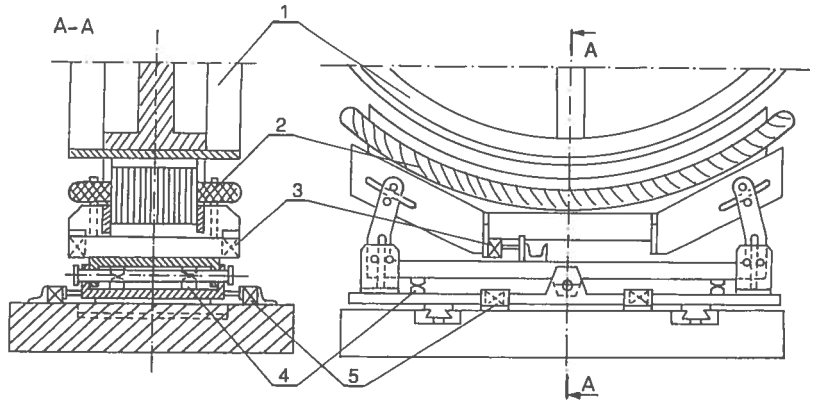

FIG. 9.7. Location of load cells for measurement of thrust, normal, and vertical forces in a test facility with rotating wheel: 1 — wheel, 2 — primary, 3 — load cells for thrust, 4 — load cells for normal force, 5 — load cells for lateral force.

The steady-state thrust can also be measured using a rotary d.c. machine with additional bearings for its stator. The shafts of a rotary machine and rotating wheel (disc) are coupled mechanically. The stator of the rotary machine is allowed to rotate freely about the axis of the shafts. So, when used as a brake, the rotating machine with additional bearings operates as a pendulum which can be scaled in newtonmetres. When the stator of the rotary d.c. machine is not equipped with bearings, the thrust under steady-state conditions can be calculated from the output of the d.c. machine.

9.4 Mesurement of velocity

The velocity must be measurered when a LIM is tested in a laboratory or is controlled using a closed loop. The linear velocity can be measured: (a) directly, with the aid of *linear tachogenerators or encoders*, or (b) indirectly, with the aid of *rotary tachogenerators or encoders*. Indirect methods are used in test facilities with rotating wheels, where a tachogenerator or

encoder is connected to the shaft and in test facilites with translatory motion or closed-loop drives, where the shaft of a tachogenerator or encoder is driven by the moving primary or secondary via a nonsliding contact (friction gear or rack-and-pinion). Any backlash between the tachogenerator shaft and rack rail affects the measurement accuracy and is not permissible, e.g. in the case of a vector-controlled LIM. Both induction and permanent magnet tachogenerators can be used as anolog speed sensors. While digital encoders may be made for linear applications, rotary encoders are more common. They consist of a disc or drum with a digitally coded scale. Such discs are manufactured with diameters from 50 to 250 mm. An *absolute encoder* is a position verification device that provides unique position information for each shaft location. The location is independent of all other locations, unlike the *incremental encoder*, where a count from a reference is required to determine position. Incremental encoders give between 100 and 50 000 pulses per 360^0. The resolution for testing LIMs should be at least 2 000 pulses/rev. For reliability, it is desirable to have discs constructed from metal rather than glass.

9.5 Measurement of electrical quantities

9.5.1 *Voltage and current*

For voltage and current measurements, *digital meters* with a frequency response that is adequate for the range 10 Hz to 20 kHz should be used. For testing low-frequency LIMs, e.g. for elevator drives, the minimum frequency should be even lower (5 Hz). LIMs are usually fed with distorted waveforms so high-frequency time harmonics should be included. When measurement of fundamental voltage is required, a *low-pass filter* with sharp cut-off characteristics is useful.

It is important to display the nonsinusoidal waveforms in the frequency domain. A visual display of the Fourier components of a given waveform against frequency can be produced using a *spectrum analyser*. Modern spectrum analysers sample and store input signals, analyse them using fast Fourier transform, display them on screen, and print out a hard copy. RS-232C or GPIB interface is common. The oscilloscope and the spectrum analyser come from the same family of general-purpose instruments. However, the spectrum analyser outclasses the oscilloscope since it can represent the signals in both the time and frequency domains, while the oscilloscope can only work in the time domain.

9.5.2 *Power*

A *digital power meter* should be adjusted for accurate power measurement of distorted waveforms. Three-phase rather than single-phase power me-

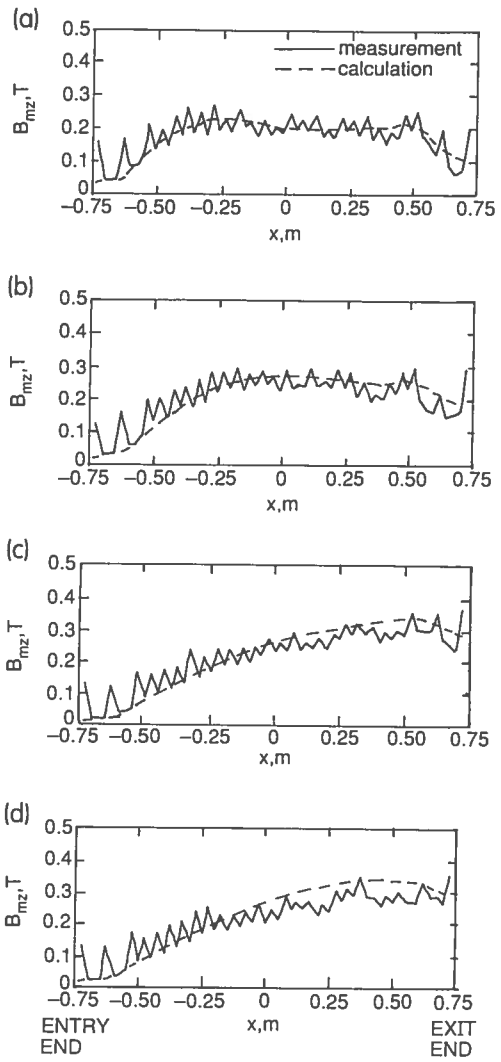

FIG. 9.8. Longitudinal distribution of the normal component of magnetic flux density in the airgap (25 Hz, 447 V) of the Kyushu University LIM according to Nonaka *et al*: (a) $s = 0.5$, (b) $s = 0.3$, (c) $s = 0.1$, (d) $s = -0.2$.

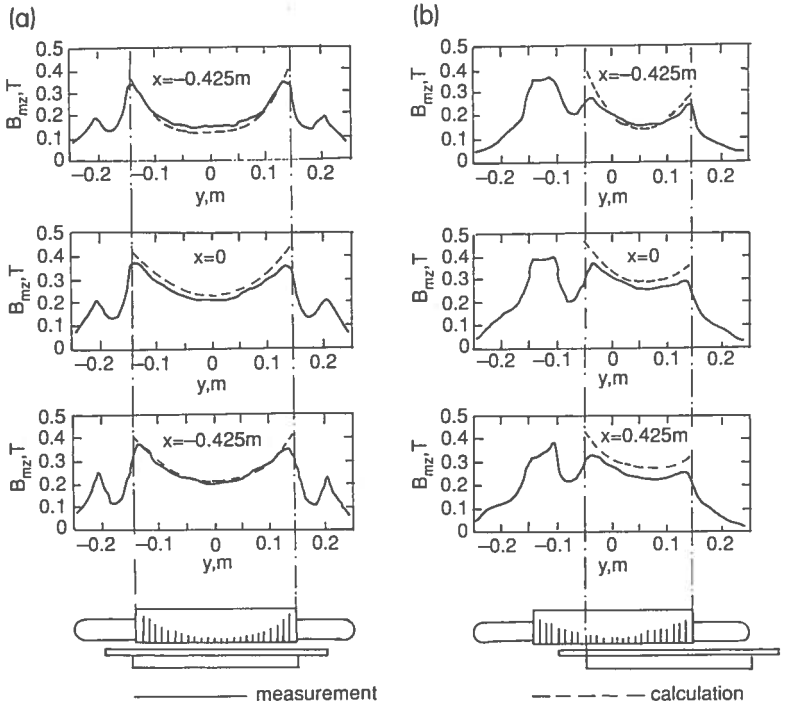

FIG. 9.9. Transverse distribution of the normal compenent of magnetic flux density in the airgap of the Kyushu University LIM (25 Hz, 135 A) according to Nonaka *et al*: (a) at normal position of the secondary, (b) at lateral displacement of 0.1 m.

ters are preferred because thay can be connected both to three-wire and four-wire circuits. Modern digital power meters incorporate easy-to-use, versatile computing functions, and provide direct digital reading of the active, reactive, and apparent power, power factor, and more. Typical features are: 0.1% accuracy, frequency range from 10 Hz to 20 kHz, analog output, RS-232C or GPIB interface, and low-pass filter.

9.6 Measurement of magnetic flux density

Gauss meters with a *germanium Hall generator* or *search coil* are used for measurement of the magnetic flux density distribution in the airgap of a LIM. The most important is the normal component (perpendicular to the active surfaces) of the magnetic flux density producing the thrust.

Kyushu University research group [122] recommends three sizes of coil of the length equal to the primary core length and of different coil spans for measurement of the normal component of the airgap magnetic flux density. The first set of search coils, with span equal to the width of the primary tooth, is wound on top of each tooth. In the next set of search coils, embracing every slot pitch, the coil span is equal to the width of slot pitch. The coil span of the last set of search coils is equal to one pole pitch. The longitudinal distribution of the normal component of the airgap magnetic flux density [107, 122] is shown in Fig. 9.8. To measure the distribution of the normal component of the airgap magnetic flux density along the bars, groups of search coils can be set at any longitudinal position. The transverse distribution of the normal component of the airgap magnetic flux density [107, 122] is shown in Fig. 9.9.

Measurement of the airgap magnetic flux density distributions allows for the evaluation of both the longitudinal end effect and the transverse edge effect.

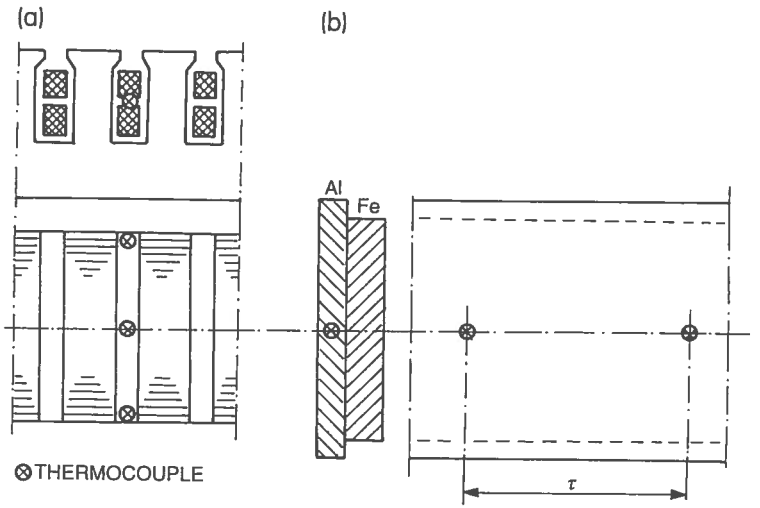

FIG. 9.10. Location of thermocouples for temperature measurement: (a) of the primary winding, (b) of the double-layer secondary.

9.7 Measurement of temperature

The temperature of the primary winding is measured using *thermocouples* inserted between the upper and lower coils in the slot. Thermocouples are installed in the centre position of the primary, half-way between each end. Three thermocouples are usually used: one in the middle of the bar and two at each end of the bar (Fig. 9.10a.)

The temperature of the reaction rail is also measured with the aid of thermocouples. It is recommended that two thermocouples be installed in the centre of the aluminium cap, allowing for one pole pitch distance between them (Fig. 9.10b). The rules for the cage secondary are the same as those for the primary winding. In test facilities with rotating wheels the output is obtained from the inside of the shaft via slip rings with high-quality contacts.

9.8 Measurement of vibration

Where the vibration forces or responses are measured during operation of the machine under test, such measurement is called simply *vibration measurement* or *vibration monitoring*. The type of test in which the structure or component is vibrated with a known excitation, e.g. using a shaker, often outside its normal service environment, is called *modal testing*. Owing to the rigid structure of a LIM, the vibration monitoring is sufficient in most cases.

Basic components of a vibration measurement system are shown in Fig. 9.11. The piezoelectric type of transducer is by far the most popular and widely-used transducer. Three types of piezoelectric transducers are available for mobility measurements: force gauges, accelerometers, and impedance heads. The *force transducer* is the simplest type of piezoelectric transducer. The transmitted force, or a known fraction of it, is applied directly across the crystal, which thus generates a corresponding electrical charge. In an *accelerometer*, transduction is indirect and is achieved using an auxiliary, or seismic mass. The output of the transducer is proportional to the acceleration of its body ($\ddot{z}$). It has been found convenient for some applications to combine both force and acceleration measuring elements in a single housing, forming an *impedance head*. The main reason for using such a device is to facilitate the measurement of both parameters at a single point. The correct location and attachement of transducers, especially accelerometers, is very important. One of the advantages of the piezoelectric transducer is that it is an active device and does not require a power supply. On the other hand, amplifiers are required which are necessary to boost the very small electrical charge that is generated by the crystals into a signal that is strong enough to be measured by the analyser.

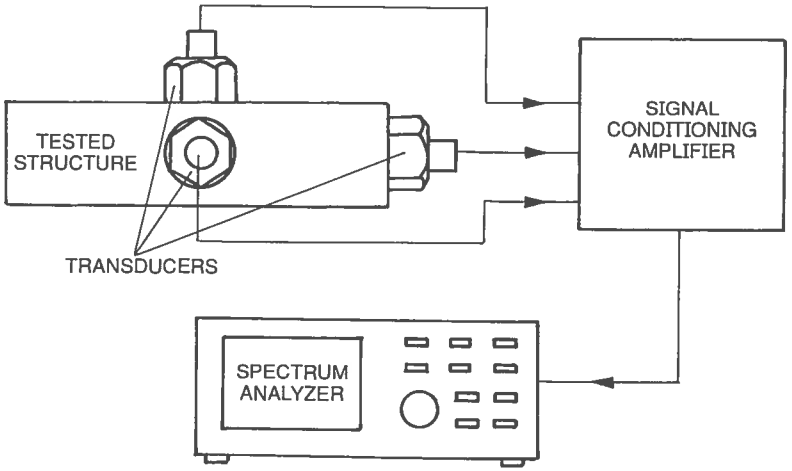

FIG. 9.11. Typical instrumentation system for vibration measurement.

In order to measure the specific parameters of interest, an *analyser* is incorporated. The oldest type of analyser is the *tracking filter*, and the most sophisticated is the *digital spectrum analyser*. Instead of using an analyser, signals from amplifiers can be sent to the A/D converter of a PC-based data acquisition system (Section 9.2).

9.9 Equivalent circuit parameters

9.9.1 *d.c. primary resistance*

An exact value of the primary resistance R_{1dc} at the d.c. supply can be obtained by measuring the d.c. voltage between winding terminals (each line-to-line or phase) and the d.c. current corresponding to the rated a.c. current. The d.c. resistances of three-phases are, in general, different.

9.9.2 *Open-secondary circuit test*

The a.c. primary winding resistance and leakage reactance can be obtained by disconnecting the secondary branch of the equivalent circuit (Fig. 3.16). Since the no-load slip of a LIM is much higher than that of its rotary counterpart, a classical 'no-load test' cannot be used. Two other methods can be applied for disconnecting the secondary branch:

(a) driving the tested LIM at synchronous speed ($s = 0$) with the aid of a second motor fed from a variable-frequency source;

(b) removing the secondary winding by replacing the real secondary with a laminated ferromagnetic core of the same dimensions and retaining the same airgap.

The second method, performed at standstill, is easier to apply since in the case of single-sided LIMs, the same second primary unit with open windings can be utilized. In the case of double-sided LIMs it is sufficient to remove the nonferromagnetic reaction rail. The input power P_{1o} (consumed by the three phases), the phase voltage V_1, phase current I_{1o}, and input frequency f should be measured. The voltage and current must be measured in all three phases to detect any phase unbalance. The input voltage should be set at the level of the rated voltage, i.e. $V_1 = V_{1r}$. The a.c. primary resistance R_1 and the resistance R_o (in series) expressed by eqn (3.114), is

$$R_1 + R_o = \frac{V_1}{I_{1o}} \cos \phi_o \tag{9.1}$$

where

$$\cos \phi_o = \frac{P_{1o}}{m_1 V_1 I_{1o}} \tag{9.2}$$

Similarly, the primary leakage reactance X_1 and the reactance X_o (in series) expressed by eqn (3.114), is

$$X_1 + X_o = \frac{V_1}{I_{1o}} \sqrt{1 - \cos^2 \phi_o} \tag{9.3}$$

Since the exciting current $I_{exc} = I_{1o}$, the core loss current I_{Fe} and the magnetizing current I_ϕ are

$$I_{Fe} = I_{1o} \cos \phi_o; \qquad I_\phi = I_{1o} \sqrt{1 - \cos^2 \phi_o} \tag{9.4}$$

The primary core losses are

$$\Delta P_{1Fe} \approx 0.5(P_{1o} - m_1 I_{1o}^2 R_{1dc}) \tag{9.5}$$

The coefficient 0.5 takes into account the presence of the auxiliary laminated core when a single-sided LIM is tested. For double-sided LIMs this coefficient is equal to unity.

The parallel and series resistances representing the primary core losses are

$$R_{Fe} = \frac{\Delta P_{1Fe}}{m_1 I_{1Fe}^2}; \qquad R_o = \frac{\Delta P_{1Fe}}{m_1 I_{1o}^2} \tag{9.6}$$

The a.c. current primary resistance is

$$R_1 \approx \frac{V_1}{I_{1o}} \cos \phi_o - R_o \tag{9.7}$$

The primary leakage reactance X_1 cannot be measured directly. First, the mutual (airgap) reactance X_g given by eqns (3.116) and (8.39) must be found. If $R_{Fe} \gg X_g$ ($R_o \ll X_o$) the reactance X_o is approximately equal to the mutual reactance X_g, which can be calculated with reasonable accuracy using eqn (8.39), in which $k_{sat} \approx 1$. Thus, the primary leakage reactance is

$$X_1 \approx \frac{V_1}{I_{1o}} \sqrt{1 - \cos \phi_o} - \frac{R_{Fe}^2 X_g}{R_{Fe}^2 + X_g^2} \tag{9.8}$$

Finally, the parallel core loss resistance can be determined again as

$$R_{Fe} = R_o + \frac{X_o^2}{R_o} \approx R_o + \frac{X_g^2}{R_o} \tag{9.9}$$

The end effect impedance $\mathbf{Z}_e$ has not been included since the test has been performed at standstill ($\mathbf{Z}_e \to \infty$).

9.9.3 *Blocked-secondary test*

When the resistances R_1, R_{Fe} and the reactances X_1, X_g are known, the secondary resistance $R_2'(s = 1)$ and the secondary reactance $X_2'(s = 1)$ can be determined by performing the blocked-secondary test with the real reaction rail (containing the closed electric secondary circuit). The input power P_{1sh} (absorbed by all three phases), input voltage V_1, and input current I_{1sh} are measured. The subscript 'sh' means 'short circuit' since the blocked secondary test on a LIM corresponds to the short-circuit test on a transformer. If the test has been performed under rated voltage $V_1 = V_{1r}$, the primary winding losses, the secondary losses, and the stray losses at $s = 1$ are

$$\Delta P_1 + \Delta P_2 + \Delta P_{str} = P_{1sh} - \Delta P_{1Fe} \tag{9.10}$$

where the primary core losses ΔP_{1Fe} have been obtained in preceding test.

The power factor at $s = 1$ is

$$\cos\phi_{sh} = \frac{P_{1sh}}{m_1 V_1 I_{1sh}} \tag{9.11}$$

Owing to the large airgap, the vertical branch current is much higher than that in a rotary induction motor, so that the vertical branch cannot be neglected at s=1. The vertical branch and the secondary branch resistance and reactance, in parallel, are:

$$R_t = \frac{V_1}{I_{1sh}} \cos\phi_{sh} - R_1 \tag{9.12}$$

$$X_t = \frac{V_1}{I_{1sh}} \sqrt{1 - \cos^2\phi_{sh}} - X_1 \tag{9.13}$$

where $R_t = \Re e[\mathbf{Z}_t]$, $X_t = \Im e[\mathbf{Z}_t]$, and $\mathbf{Z}_t$ is according to eqn (3.117). Eqn (3.117) allows separation of the secondary resistance and reactance at standstill:

$$R'_2(s=1) = \Re e[\mathbf{Z}'_2(s=1)]$$

$$= \frac{(R_t R_o - X_t X_o)(R_o - R_t) + (X_t R_o + R_t X_o)(X_o - X_t)}{(R_o - R_t)^2 + (X_o - X_t)^2} \tag{9.14}$$

$$X'_2(s=1) = \Im e[\mathbf{Z}'_2(s=1)]$$

$$= \frac{(X_t R_o + R_t X_o)(R_o - R_t) - (R_t R_o - X_t X_o)(X_o - X_t)}{(R_o - R_t)^2 + (X_o - X_t)^2} \tag{9.15}$$

where

$$\mathbf{Z}'_2(s=1) = \frac{\mathbf{Z}_o \mathbf{Z}_t}{\mathbf{Z}_o - \mathbf{Z}_t} \tag{9.16}$$

and $\mathbf{Z}_o$, R_o, and X_o are according to eqns (3.112) and (3.114), and have been determined in the preceding test.

Note that only for the cage secondary of a single-sided LIM and very thin nonferromagnetic secondary of a double-sided LIM does $R'_2/s \approx R'_2(s=1)/s$ and $X'_2 \approx X'_2(s=1) \approx const.$ For a LIM with a double-layer secondary (aluminium cap over back iron) the secondary resistance and leakage reactance are complicated functions of slip (Section 4.2) and should be determined separately for each value of the velocity.

The starting thrust is

$$F_{st} = \frac{m_1}{v_s} (I'_2)^2 R'_2(s=1) \tag{9.17}$$

where

$$I'_2 = \frac{E_1}{\sqrt{[R'_2(s=1)]^2 + [X'_2(s=1)^2]}} \tag{9.18}$$

$$E_1 = \frac{\sqrt{R_t^2 + X_t^2}}{\sqrt{(R_1 + R_t)^2 + (X_1 + X_t)^2}} V_1 \tag{9.19}$$

REFERENCES

1. Alscher, H., Boldea, I., Eastham, A.R., and Iguchi, M. (1984). Propelling passengers faster than a speeding bullet. *IEEE Spectrum*,**8**, 57–64.
2. Alwash, J.H.H. and Eastham, J.F. (1976). (Permeance harmonics analysis of short-stator machines. *Proceedings IEE*,**123**, No. 12, 1335–40.
3. Alwash, J.H.H. and Al-Rikabi, J.A.H. (1979). Finite element analysis of linear induction machines. *Proceedings IEE*,**126**, No. 7, 677–82.
4. Bailey, A.R. and Edgar, J.P. (1974). The use of linear motors in textile shuttle propulsion. *IEE Conf. Publ.*,**120**, 101–5.
5. Berndt, P., Kroger. U., and Saumwebber, E. (1979). The principles of operation of track brakes (magnetic and eddy-current) — interaction with the track. *Int. Conf. on Railway Braking*, IMechE, York, 229–42.
6. Bevan, R.J.A. and Kalman, G. (1979). Non-uniform power distribution in linear induction motors due to end effects. *IEEE Trans. on Power Apparatus and Systems*,**PAS-98**, No. 5, 1516–21.
7. Białous Z. (1980). Problems related to electromagnetic calculations of motors of series F (in Polish). *Prace Instyt. Elektrot.*, Warsaw,**21**, 21–36.
8. Bianu, A., Gavril, S., and Schieber, D. (1979). Speed regulation of a linear motor with disk-rotor by radial displacement of stator. *Conf. Special Purpose Elec. Machines*, Bydgoszcz, 9–15.
9. Bočarov, V.I. and Nagorsky, V.D. (1985). *High-speed ground transport with linear propulsion and magnetic suspension system* (in Russian). Transport, Moscow.
10. Boldea, I. and Babescu, M. (1976). Multilayer theory of dc linear brakes with solid iron secondary. *Proceedings IEE*,**123**, No. 3, 220–2.
11. Bolton H. (1969). Transverse edge effects in sheet-rotor induction motors. *Proceedings IEE*,**116**, 725–31.
12. Bose, B.K. (1985). Sliding-mode control of induction motor. *IEEE/IAS Annual Mtng*,**21B**, 479–486.
13. Bose, B.K. (1986). *Power electronics and ac drives*. Prentice Hall, Englewood Cliffs.
14. Brunelli, B., Casadei, G., and Tani. A. (1991). T-shaped LIM driven by a three-phase PWM ac chopper. *4th European Conf. EPE'91*, Florence, **1**, 481–486.
15. Budig, P.K., Timmel, H., Hofman, J., Peschke, K., Schuffenhauer, U., and Zeumann, R. (1991). A new drive for the micrometer- and submicrometer-range. *4th European Conf. EPE'91*, Florence, **1**, 510–14.
16. Cecconi, V., Nuccio, S., and Serporta, C. (1981). Laboratory investigations of a large-scale linear motor (in Italian). *L'Energia Elettrica*, **58**, No. 11, 3-7.
17. Cecconi, V., Nuccio, S., Ricco Galluzzo, G., and Serporta, C. (1988). Experimental investigation of inverter-fed single-sided linear induction motor. *Int. Conf. ICEM'88*, Pisa, **2**, 171–175.
18. Chalmers, B.J., Spooner, E., and Abdel-Hamid, R.H. (1980). Parameters of solid-rotor induction machines with unbalanced supply. *Proceedings IEE Pt B*, **127**, No. 3, 174–82.
19. Choudhury, P., Dawson, G.E., Eastham, A.R., John, V.I., and Parker, J.H. (1989). Non-contact energy transfer to automobiles. *Int. Conf. Maglev'89*, Yokohama, 179–84.
20. Coho, O.C., Kliman, G.B., and Robinson, J.I. (1974). Experimental evaluation of a high speed double-sided linear induction motor. *IEEE/PES Summer Mtng*, Anaheim, 10–17.
21. Dawson, G.E. and Eastham, A.R. (1981). The comparative performance of single-sided linear induction motors... . *16th IEEE/IAS Mtng*, Philadelphia, **81CH1678-2**, 323–9.
22. Dawson, G.E., Eastham, A.R., Gieras, J.F., Ong, R., and Ananthasivam K. (1986). Design of linear induction drives by field analysis and finite-element technique. *IEEE Trans. on Industry Applications*,**IA-22**, 865–73.
23. Dombrovsky, V.V. and Khutorietsky G.M. (1974) *Principles of design of ac electrical machines* (in Russian). Energia, St Petersburg.
24. Eastham, J.F. and Balchin, M.J. (1974). Pole-change windings for linear induction motors. *Proceedings IEE*,**122**, No. 2, 154–60.
25. Eastham, A.R., Dawson, G.E., Gieras, J.F., Ong, R., and Ananthasivam, K. (1987). Comparison of calculation results of a single-sided LIM using finite element and circuital methods (in Polish). *Przegląd Elektrot.*, No. 4, 81–85.
26. Fintescu, N.D. and Pascal J.P. (1986). Tests results of full-scale 1MW linear induction motor (U-LIM-as) with PWM inverter. *Int. Conf. Maglev and Linear Drives*, Vancouver, 165–70.
27. Fleszar, J. and Mendrela, E.A. (1983). Twin-armature rotary-linear induction motor. *Proceedings IEE*,**130**, No. 3, 186–92.
28. Freeman, E.M. (1968). Travelling waves in induction machines: input impedance and equivalent circuits. *Proceedings IEE*,**115**, No. 12, 1772–6.
29. Furukawa, T., Muta, I., Komiya, K., Nonaka, S., and Ogawa, K. (1987). Finite element analysis of a linear induction motor travelling in a metal tube. *Elec. Energy Conf.*, Adelaide, 467–72.

30. Gibbon, M.A. and Parker, J.H. (1986). Operational experience with a LIM driven transit system. *Int. Conf. Maglev and Linear Drives*, Vancouver, 135–9.
31. Gibbs, W.J. (1946). Theory and design of eddy current slip couplings. *BEAMA Journal*,**53**, 123–219.
32. Gieras, J.F. (1977). Analytical method of calculating the electromagnetic field and power losses in ferromagnetic halfspace, taking into account saturation and hysteresis. *Proceedings IEE*,**124**, No. 11, 1098–104.
33. Gieras, J.F. (1977). Theory of induction machines with double-layer secondary. *Rozprawy Elektrot.*,**23, No. 3**, 577–631.
34. Gieras, J.F. (1979). Contribution to the field analysis of induction machines with cage rotor (in Polish). *Conf. Special Purpose Elec. Machines*, Bydgoszcz, 87–104.
35. Gieras, J.F. (1982). Linear induction motor with transverse flux in electrodynamic levitation systems. *Int. Conf. ICEM'82*, Budapest, 980–3.
36. Gieras, J.F. (1982). Electrodynamic forces in electromagnetic levitation systems. *Acta Technica ČSAV*, No. 5, 532–45.
37. Gieras, J.F. (1983). Simplified theory of double-sided linear induction motor with squirrel-cage elastic secondary. *Proceedings IEE Pt B*,**130** No. 6, 424–30.
38. Gieras, J.F. (1984). Influence of structure and material of the secondary suspended... . *etzArchiv*,**6**, No. 7, 255–60.
39. Gieras, J.F. (1984). Equipment for testing flat single-sided linear induction machines (in Polish). *Przegląd Elektrot.*, No. 3, 84–9.
40. Gieras, J.F. (1985). Three- dimensional multilayer theory of induction machines and devices. *Acta Technica ČSAV*, No. 5, 525–48.
41. Gieras, J.F. (1985). Analysis of single-sided linear induction motor using an equivalent circuit with longitudinal end effect taken into account. *etzArchiv*,**7**, 405–8.
42. Gieras, J.F. (1985). Transverse flux electrodynamic levitation systems. *Int. Conf. Maglev Transport'85*, Tokyo, 207–15.
43. Gieras, J.F. (1988). Two phase rotary-linear induction motor for propulsion of robot end-effector. *Int. Conf. ICEM'88*, Pisa, **2**, 165–9.
44. Gieras J.F. (1989). The aspects of design of single-sided linear induction motors ... . *Int. Conf. MAGLEV'89*, Yokohama, 321–6.
45. Gieras J.F. (1990). Sizing equations and magnetic circuit design for single-sided LIMs. *Int. Conf. ICEM'92*, MIT Cambridge, 498–503.
46. Gieras J.F. (1990). Design strategy of linear induction drives for industrial applications. *Elec. Drive Symp. EDS'90*, Capri, 285–90.
47. Gieras J.F. (1990). *Linear induction motors* (in Polish). WNT, Warsaw.

48. Gieras, J.F. (1991). Analysis of multilayer rotor induction motor with higher space harmonics taken into account. *Proceedings IEE Pt B*,**138**, 32–6.
49. Gieras J.F. (1993). Seizing equations for single-sided linear induction motors. *Elec. Machines and Power Systems*, **21**, 25–37
50. Gieras J.F. (1992). Calculation of stray losses in a single-sided linear induction motors. *Archiv für Elektrotechnik*, **75**, 103–7.
51. Gieras, J.F. and Hochhäusler, P. (1983). Investigations into Maglev Transport (in Polish). *Przegląd Elektrot.*, No. 6, 236–9.
52. Gieras, J.F., Eastham, A.R., and Dawson, G.E. (1985). Performance calculation for single-sided linear induction motors with a solid steel reaction plate... . *IEE Proceedings Pt B*,**132**, 185–194.
53. Gieras, J.F., Eastham, A.R., and Dawson, G.E. (1985). The influence of secondary solid ferromagnetic plate thickness on the performance ... . *Elec. Machines & Power Systems*,**10**, 67–77.
54. Gieras, J.F., Eastham, A.R., and Dawson, G.E. (1985). Influence of phase unbalance on the thrust of a single-sided LIM. *2nd Int. Conf. on Elec. Machines*, IEE, London, 304–8.
55. Gieras, J.F., Dawson, G.E., and Eastham, A.R. (1986). Performance calculation for single- sided linear induction motors with a double-layer reaction rail... . *IEEE Trans. on Magnetics*,**MAG-22**, 54–62.
56. Gieras, J.F., Eastham, A.R., and Dawson, G.E. (1986). The influence of conductive cap thickness on the performance of single-sided linear induction motors. *Elec. Machines and Power Systems*,**11**, 125–36.
57. Gieras, J.F., Eastham, A.R., Dawson, G.E., and Ballantyne, W.J.(1986). Approach to performance calculation of a single-sided LIM with a cage reaction rail. *Int. Conf. on Maglev and Linear Drives*, Vancouver, 187–92.
58. Gieras, J.F., Dawson, G.E., and Eastham A.R. (1987). A new longitudinal end effect factor for linear induction motors. *IEEE Trans. on Energy Conversion*,**EC-2**, 152–9.
59. Gieras, J.F. and Hochhäusler, P. (1987). Electromagnetic field and forces in salient-pole LIMs ... . *Int. Symp. ISEF'87*, Pavia, 145–8.
60. Gieras, J.F., Eastham, A.R., and Dawson, G.E. (1988). An evaluation of the effect of varying the side bar cross section ... . *Int. Conf. ICEM'88*, Pisa, **2**, 159–64.
61. Gieras, J.F., Eastham, A.R., Dawson, G.E. and John, G. (1990). Calculation of thrust for a single-sided linear induction motor, taking into account phase unbalance and higher time harmonics. *Archiv für Elektr*,**73**, 299–308.
62. Gieras, J.F., Kleinhans, P., Manchen, M.L., and Voss, E. (1992). Experimental investigations of a shaded-pole flat linear induction motor. *Int. Conf. Africon'92*, Swaziland, 404–8.

63. Graczyk, M. and Mrugała, B. (1976). Cooling of flat linear motors SL-5. (in Polish). *Maszyny Elektr – ZP*, Katowice, **24**, 69–72.
64. Guderjahn, C.A., Wipf, S.I., Fink, H.J., Boom, R.W., MacKenzie, K.E., Williams, D., and Downey, T. (1969). Magnetic suspension and guidance for high speed rockets by superconducting magnets. *Journal of Appl. Physics*, **40**, No. 5, 2133–40.
65. Guterl, F. and Truxal, C. (1982). The wonderful world of Epcot. *IEEE Spectrum*, **9**, 46–54.
66. Hamels, D. and Compter, J.C. (1985). Performance comparison of various electromagnetic actuators. *Symp. on Electromechanics ...*, S. Felice Circeo, Latina, 239–48.
67. Hannkam, L. (1965).Wirbelströme in dünnen leitenden Platten infolge bewegter stromdurchflossener Leiter. *ETZ-A*,**86**, No. 13, 427–431.
68. Heller, B. and Hamata, V. (1977). *Harmonic field effects in induction machines* Elsevier, Amsterdam.
69. Hosny, W.M., Dodds, S.J., and Annaz, F.Y. (1990). Sliding mode control of the rotary tubular induction motor. *Elec. Drives Symposium EDS'90*, Capri, 31–35.
70. Isamuhamedov, Z.S. and Khadjinova, M.U. (1986). *Multirotor asynchronous motors for cotton combines* (in Russian). FAN, Tashkent.
71. Izelia, G.I., Rebrov, S.A., and Shapovalenko, A.G. (1975). *Linear induction motors* (in Russian). Tekhnika, Kyiev.
72. Kamiński, G., Kant, M., and Virolleau, A. (1978). A study of linear rotating motor. *Int. Conf. ICEM'78*, Brussels, **L3**, 2/1–2/24.
73. Kawanishi, T., Takagi, N., Kato, W., Karita, J., and Takakado, Y. (1989). Testing machine of hydrodynamic forces using linear motor. *Int. Conf. Maglev'89*, Yokohama, 351–6.
74. Kliman, G.B., Mischler, W.R., and Oney, W.R. (1980). Performance of a single-sided linear induction motor with solid back iron and with various misalignments. *GEC Report*, Schenectady, FRA/ORD-80/53–1.
75. Komęza, K., Wiak, S. and Rakoczy, Z. (1983). Investigations into the dynamics of a LIM-driven hoist (in Polish). *Elektryka TU Łódź*,**74**, No. 432, 347–56.
76. Kordecki, A. and Węgliński, B. (1988). Tubular linear motors made of iron matrix powder composites. *Int. Conf. ICEM'88*, Pisa, **2**, 133–8.
77. Kortüm, W. (1984). Vehicle response on flexible track. *Int. Conf. Maglev Transport*, Solihull, 47–58.
78. Koseki, T., Morizane, T., Ohsaki, H., and Masada, E. (1991). Novel linear induction drives: control scheme and converters. *4th European Conf. EPE'91*, Florence, **1**, 481-6.
79. Laithwaite, E.R. (1966). *Induction machines for special purposes.* G. Newnes Ltd, London.

80. Laithwaite, E.R. (1970). *Propulsion without wheels.* The English Universities Press Ltd, London.
81. Laithwaite, E.R. (1971). *Linear electric motors* Mills & Boon Ltd, London.
82. Lammeraner, J. and Štafl, M. (1964). *Eddy Currents.* Iliffe Books Ltd, London.
83. Laugis, J.J. (1982). Linear induction motor with two efficient outputs. *Int. Conf. ICEM'82*, Budapest,**2**, 1006–8.
84. Linacre, H. (1984). Birmingham Airport maglev propulsion system. *Int. Conf. Maglev Transport*, Solihull, 1193–201.
85. Loron, L. and Peters, G.H.L. (1991). Application of an extended Kalman filter to the estimation of the parameters of a solid rotor asynchronous drive ... . *4th European Conf. EPE'91*, Florence, **3**, 532–7.
86. Löser, F., Ruoss, W., and Sattler, P.K. (1988). Eddy-current brake system for Transrapid 07. *Int Conf. Maglev Systems*, Hamburg, 175–184
87. Marshall, S.V. and Skitek G.G. (1987). *Electromagnetic concepts and applications* (second edition). Prentice Hall Inc., Englewood Cliffs, NJ.
88. Menden, W., Mayer, W.J., and Rogg, D. (1989). State of development and future prospects on the Maglev systems... . *Int. Conf. Maglev'89*, Yokohama, 11–18.
89. Mendrela, E.A. and Gierczak, E. (1987). Double-winding rotary-linear induction motor. *IEEE Trans. on Energy Conv.*,**EC-2**, No. 1, 47–54.
90. Mendrela, E.A. and Turowski, J. (1978). Rotary-linear induction motor. *IEEE Winter Power Mtng*, NY, A78 091–1.
91. Miller, L. and Ruoss, W. (1989). Performance analysis of the Transrapid 07. *Int. Conf. Maglev'89*, Yokohama, 85–92.
92. Money, L.J. (1984). *Transportation, energy and the future.* Prentice Hall Inc., Englewood Cliffs, NJ.
93. Müller, F. (1977). Induktionsverlaufe und Wirbelstromverteilung bei asynchronen Linearmotoren; Messegebnisse. *Elektrotechnik und Maschinenbau*,**94**, 151–4.
94. Nagaike, T. and Takatsuka, H. (1989). Present status and prospect of HSST. *Int. Conf. Maglev'89*, Yokohama, 29–35.
95. Nasar, S.A. and Boldea, I. (1976). *Linear motion electric machines.* J. Wiley & Sons, NY–London–Sydney–Toronto.
96. Neyman, L.R. (1949).*Skin effect in ferromagnetic bodies.* (in Russian). Energia, St Petersburg.
97. Nishiki T. (1985). Running track of the linear car. *Int. Conf. Maglev Transport'85*, Tokyo, 319–324.
98. Nitka, S. (1976). *Electromechanical energy conversion in linear asynchronous machines* (in Polish). Śląsk (PZKMPW), Katowice.

99. Nitka, S. (1976). Approximate calculation resistances and reactances of flat linear induction motors (in Polish). *Maszyny Elektr – ZP*, Katowice, **24**, 33–7.
100. Nitka, S. (1979). Operation of three-phase flat linear induction motors on a single-phase network (in Polish). *Conf. Special Purpose Elec. Machines*, Bydgoszcz, 29–32.
101. Nonaka, S. and Yoshida, K. (1971). Characteristics of linear motors with sandwich compound conducting plates. *Elec. Eng. in Japan*,**91**, No. 1, 183–93.
102. Nonaka, S. and Fuji, N. (1982). Performance of double-sided high-speed LIM with a hollow aluminium reaction rail. *Int. Conf. ICEM'82*, Budapest, 984–7.
103. Nonaka, S. and Higuchi, T. (1982). Approximate equations for calculation of characteristics of single-sided linear induction motors. *Elec. Eng. in Japan*,**102**, 18–25.
104. Nonaka, S. and Higuchi, T. (1986). Design of single-sided LIMs for urban transit. *Int. Conf. Maglev & Linear Drives*, Vancouver, 141–8.
105. Nonaka, S. and Higuchi, T. (1987). Design strategy of single-sided linear induction motors for propulsion of vehicles. *Int. Conf. Maglev & Linear Drives*, Las Vegas, 1–5.
106. Nonaka, S. and Higuchi, T. (1988). Reduction of vertical force of single-sided linear induction motor for urban transit. *Int. Conf. on Maglev Systems*, Hamburg, 121–9.
107. Nonaka, S., Fuji, N., Watanabe, T., and Kojima, Y. (1988). Examination with test facility on dynamic characteristics of LIM for urban transit. *Int. Conf. ICEM'88*, Pisa, **2**, 127–32.
108. Nonaka, S. and Higuchi, T. (1989). On the reduction of energy consumption of linear induction motors in urban transit. *Int. Conf. Maglev'89*, Yokohama, 333–8.
109. Oberretl, K. (1974). Einseitiger Linearmotor mit Käfig Sekundäteil. *Archiv für Elektrotechnik*,**56**, No. 6, 305–19.
110. Oberretl, K. (1976). Testing and calculation of the American high-speed linear motor of Pueblo, Colorado. *2nd Int. Conf. on Hover Crafts...*, Amsterdam, 45–50.
111. Ohishi, A. (1989). HSST-05 system — General and operational outline at YES'89. *Int. Conf. Maglev'89*, Yokohama, 93–100.
112. Ohsaki, H., Masada, E., and Henneberger, G. (1992). Design of linear induction motor for the control of conductive fluid flow. *Int. Conf. ICEM'92*, Manchester, **2**, 716–20.
113. Panasenkov, M.A. (1971). *Electromagnetic calculations of devices with nonlinear distributed parameters* (in Russian). Energia, Moscow.
114. Pascal, J.P. (1989). The Starlim Maglev. *Int. Conf. Maglev'89*, Yokohama, 93–100.

115. Pawluk, K. and Szczepanski, W. (1974). *Linear electric motors* (in Polish). WNT, Warsaw.
116. Peabody F., Dunford, W.G., and Brdicko J. (1986). An analysis of a thin steel rotor, double-sided, annular LIM. *Int. Conf. Maglev and Linear Drives*, Vancouver, 193–8.
117. Picardi, A. and Romano, D. (1992). Design criteria for short stator single-sided linear induction motor ... . *Int. Symp. SPEEDAM'92*, Positano, Italy, 365–71.
118. Pietrzak, S. and Zakrzewski, K. (1983). Test facility for measurement of the steady-state characteristics of a double-sided linear motor (in Polish). *Zesz. Nauk. PL Elektryka*,**432**, No. 74, 337–45.
119. Pollard, M.G. and Riches, E.E. (1985). Birmingham Maglev: Development for the future. *Int. Conf. Maglev Transport'85*, Tokyo, 123–36.
120. Poloujadoff, M. (1980). *The theory of linear induction machinery*. Clarendon Press, Oxford.
121. Raschbichler, H.G. and Miller, L. (1992). Readiness for application of the Transrapid Maglev system. *RTR-Railway Technical Review*,**33**, 2–7.
122. Queen's University, Dept of Electrical Engineering. (1990). *Int Program on Linear Electric Drives - Package for Working Sessions at MIT* (ICEM'90). Kingston.
123. Rabiee, M. and Cathey, J.J. (1988). Verification of a field theory analysis applied to a helical motion induction motor. *IEEE Trans. on Magnetics*, **24**, No. 4, 2125–32.
124. Richter R. (1954). *Elektrische Maschinen, Band 4: Die Induktionsmaschinen* (2nd edn). Birkhäuser Verlag, Basel.
125. Richter R. (1967). *Elektrische Maschinen, Band 1: Allgemeine Berechnungselemente; Die Gleichstrommaschinen* (3rd edn). Birkhäuser Verlag, Basel.
126. Russell, R.L. and Norsworthy, K.M. (1958). Eddy currents and wall losses in screened rotor induction motors. *Proceedings IEE*,**105A**, 163–75.
127. Saleh, M.A., Ali, S.M. Sakr, M.F., and Fahim, A.A. (1979). Electric tubular motor with composite rotor. *Elec. Machines and Electromechanics*,**4**, No. 1, 47–57.
128. Sankaran, R., Pillai, K.P.P., and Muraleedharan, K.A. (1979). Voltage fed operation of linear induction motors under conditions of supply unbalance. *Proceedings IEE*,**126**, No. 4, 293–7.
129. Sattler, P.K. (1985). A 3-dimensional calculation method for a LIM having U-shaped secondary compared with measurements. *Int. Conf. Maglev Transport'85*, Tokyo, 29–35.
130. Shoyama, Y. (1984). Prototype LIM-driven railcar for subways of smaller cross section tunnels. *Japanese Railway Eng*,**24**, 11–15.

131. Shturman, G.I. (1946). Induction machines with open magnetic circuits. (in Russian) *Elektrichestvo*,**10**, 76–7.
132. Sobiczewska, G., Sosnowski, S., and Turowski, J. (1976). Dynamics of LIM-driven switching cars and cranes (in Polish). *Maszyny Elektr. – ZP*, Katowice,**24**, 38–42.
133. Sokolov, M.M. and Sorokin, L.K. (1974). *Electrical drive systems with linear asynchronous motors* (in Russian). Energia, Moscow.
134. The LIM elevator drive. (1991). *Elevator World*, No. 3, 34–41.
135. Timar, P.L., Fazekas, A., Kiss, J., Miklos, A., and Yang, S.J. (1989). *Noise and vibration of electrical machines* Elsevier, Amsterdam–Oxford–New York–Tokyo.
136. Turner, D.B. and Wolf, W.L. (1982). Houston WEDway people mover control and propulsion system. *32nd IEEE Vehicular Techn. Conf.*, San Diego.
137. Turowski, J. (1982). *Electromagnetic calculations of active parts of electrical machines and devices* (in Polish). WNT, Warsaw.
138. Verte, L.A. (1963). Experimental induction pump for liquid iron (in Russian). *Elektrichestvo*,**12**, 64–6.
139. Voldek, A.I.(1978). *Induction magnetohydrodynamic machines for transportation of liquid metals* (in Russian). Energia, St Petersburg.
140. Wallace, A.K., Parker, J.H., and Dawson, G.E. (1980). Slip control for LIM propelled transit vehicles. *IEEE Trans. on Magnetics*,**MAG-16**, 710–12.
141. Watt, D.A. (1958). The design of electromagnetic pumps for liquid metals. *Proceedings IEE*,**2763U**, 94–103.
142. Yamada, H. (1986). *Handbook of linear motor applications* (in Japanese). Kogyo Chosakai Publ. Co. Ltd.
143. Yamamura, S. (1978). *Theory of linear induction motors* (2nd edn). University of Tokyo Press, Tokyo.
144. Yamamura, T., Onuki, T., and Sekine, H. (1986). Tubular linear motor with square section. *Int. Conf. ICEM'86*, Munich, 293–63.
145. Yamamura, T., Onuki, T., Kakita, K., and Hashimoto, M. (1987). Characteristics of the tubular linear induction motor with square cross section ... . *Elec. Energy Conf.*, Adelaide, 193–8.
146. Yee H. (1971). Effects of finite length in solid-rotor induction machines. *Proceedings IEE*,**118**, 1025–33.

INDEX